# Projection of atomistic simulation data for the dynamics of entangled polymers onto the tube theory: calculation of the segment survival probability function and comparison with modern tube models†

**Pavlos S. Stephanou, Chunggi Baig* and Vlasis G. Mavrantzas***

*Received 5th May 2010, Accepted 1st July 2010*
**DOI: 10.1039/c0sm00327a**



State-of-the-art tube models for the dynamics of entangled polymer melts are usually validated on the basis of the agreement of their predictions for the linear viscoelastic properties (LVE data) of the system against experimentally measured data. We present here a more direct and fundamental test of these models based on their comparison against molecular dynamics (MD) simulation data for the dynamics of primitive paths (PPs) in the system under study. More precisely, we show how one can take advantage of a recently developed computational methodology (P. S. Stephanou, C. Baig, G. Tsolou, V. G. Mavrantzas and M. Kröger, *J. Chem. Phys*., 2010, **132**, 124904) for calculating the most important function of all tube models, the segment survival probability $\psi(s,t)$ and its average $\Psi(t)$ (the overall tube survival probability), by projecting MD data of atomistically detailed samples onto the level of the primitive paths, to directly probe mechanisms proposed for chain relaxation, such as contour length fluctuation (CLF) and constraint release (CR). The simulation data for $\psi(s,t)$ and $\Psi(t)$ can be used next to evaluate refinements of the original Doi–Edwards reptation theory based on a modified diffusion equation for $\psi(s,t)$ incorporating the terms proposed to account directly or indirectly for these effects (CLF and CR). The functions $\psi(s,t)$ and $\Psi(t)$ determined directly from the atomistic MD simulation data account automatically for all these relaxation mechanisms, as well as for any other mechanism present in the real melt. We present and discuss results from such an approach referring to model, strictly monodisperse *cis*- and *trans*-1,4-polybutadiene and polyethylene melts containing on average up to 6 entanglements per chain, simulated in full atomistic detail for times up to a few microseconds (that is, comparable to the chain disentanglement time $\tau_d$). From the same simulations we also present results for two other measures of the PP dynamics in the framework of the reptation theory, the time auto-correlation function of the PP contour length $L$ and the time auto-correlation function of the chain end-to-end vector $\mathbf{R}$. Our methodology, which serves as a bridge between molecular simulations and analytical tube theories, helps quantify chain dynamics in entangled polymers and understand how it is influenced by factors like melt polydispersity and chain molecular architecture, or the presence of interfaces. It can also be straightforwardly extended to polymeric liquids under non-equilibrium conditions (*e.g.*, subjected to a flow field) to understand the interplay between flow and entanglements.

## 1. Introduction

Dynamics in entangled polymer melts and concentrated solutions has been explained by de Gennes[1] and Doi and Edwards[2,3] by considering the effect of topological constraints on the motion of one chain by the surrounding chains, which can be effectively described by the tube model. The effective tube defines essentially the region within which the allowed conformations of the chain are confined;[4] it represents effectively all of the topological constraints acting on the chain and, since the surrounding chains are also moving, its shape also changes accordingly with time. In this picture, and in order not to violate the topological constraints, a chain is forced to execute a motion that looks very much like reptation through the tube. Reptation is therefore considered to be the dominant mechanism for chain dynamics in a system of topologically interacting molecules and if it is the only relaxation or dynamical mode, then the polymer molecule moves back and forth through the tube along its contour with a one-dimensional curvilinear diffusion coefficient $D_c$ corresponding to the overall translation of a Rouse chain.

There are two key quantities in reptation theory: the value $d_t$ of the effective tube diameter and the concept of the primitive path (PP). The former determines essentially the average strength of the topological interactions. The latter refers to the average chain conformation, at any moment, if we disregard small-scale fluctuations of the chain in and out the tube. Mathematically the PP is defined as the shortest path that connects the two ends of the

*Department of Chemical Engineering, University of Patras & FORTH-ICE/HT, Patras, GR, 26504, Greece; Web: http://lstm.chemeng.upatras.gr. E-mail: cbaig@iceht.forth.gr; Fax: +30-2610-965223; Tel: +30-2610-969515; vlasis@chemeng.upatras.gr; +30-2610-965223; +30-2610-997398*

† Electronic supplementary information (ESI) available: The potential models employed in the molecular dynamics (MD) simulations for polyethylene (PE) and *cis*-1,4 and *trans*-1,4-polybutadiene (PB) melts. See DOI: 10.1039/c0sm00327a

 

chain without violating the topological constraints and having the same topology relative to the chain itself.[5] To cast the reptation idea into a theory for polymer dynamics and then use it to develop a constitutive model for polymer melts, Doi and Edwards[2] introduced a third important quantity, the segment survival probability function $\psi(s,t)$. This represents the probability that the original tube segment $s$ remains after time $t$ or, equivalently, the probability that the primitive chain segment $s$ remains inside the original tube (the tube at time $t = 0$) after time $t$. Accordingly, the average value of $\psi(s,t)$ over all primitive chain segments, $\Psi(t)$, represents the portion of the primitive chain that remains inside the initial tube at a later time $t$, and all the linear viscoelastic properties of the polymeric systems can be determined from this.[3]

Predictions of the original theory and extensive comparisons against viscoelasticity data (*e.g.*, for the zero-shear viscosity $\eta_0$ and the chain center-of-mass diffusion coefficient $D_G$ and their dependence on chain length $N$ or chain molecular weight $M$) for entangled polymer melts compiled by several groups of investigators have shown that reptation alone is not capable of adequately describing the experimental observations.[3,6,7] For example, the original theory (developed for the simplest possible system, a chain of constant contour length in a fixed network) predicts that $\eta_0 \sim M^3$ and $D_G \sim M^{-2}$, whereas the experimental data support that $\eta_0 \sim M^{3.4}$ and $D_G \sim M^{-2.3}$.[3,6–8] Also, the dynamic loss modulus $G''(\omega)$ at intermediate frequencies $\omega$ scales as $G''(\omega) \sim \omega^{-1/2}$ whereas the experimental observations suggest a scaling of the form $G''(\omega) \sim \omega^{\alpha}$ with $-1/4 \leq \alpha \leq 0$ (although the scaling $G''(\omega) \sim \omega^{-1/2}$ is not entirely incorrect, since it can be observed at an intermediate range of frequencies in measurements with some very high molecular weight samples).[3,6,7,9–13] To correct for deviations between analytical predictions and direct experimental data, several modifications of the original Doi–Edwards theory have been proposed over recent years, namely incorporation into the tube model, in addition to reptation, of extra mechanisms for chain relaxation known today as contour length fluctuation (CLF)[14] and constraint release (CR).[7,15]

CLFs refer to the variation of the PP contour length $L$ arising naturally from the Rouse motion of primitive chain segments and also from the fluctuations in the topology of the entanglement network itself in the underlying melt structure.[14] To appraise its effect, we note that according to the refined reptation theory by Doi,[14] the ratio $\Delta L/\langle L\rangle$ of contour length fluctuations $\Delta L \equiv \sqrt{\langle L^2\rangle - \langle L\rangle^2}$ over the average value $\langle L\rangle$ decreases with $M$; thus, the CLF effect should become weaker and weaker as the chain length increases (but, still, for the finite molecular weight polymers encountered in practice, its effects should be important).[3,14] Indeed, by accounting for this, a significant improvement is observed in the comparison between theoretically predicted and measured viscoelastic data.[3,10,11,13,14,16]

CR refers to the release of the topological constraints imposed on a chain by the surrounding chains, since these are also moving with time.[7,15,17] Since new constraints will also be forming with a rate practically similar to the rate at which existing constraints are released,[11] CR should not affect the average value of the tube diameter. Given that the tube itself exhibits Rouse dynamics subject to these local rearrangements, the main effect of CR will be to cause what is termed in the literature as *tube reorganization*.[7,17–19] Being a *many-body* interaction, it is very difficult to account for CR in a rigorous manner in the tube theory, its analysis requiring detailed knowledge of the local dynamics of entanglement points (*e.g.*, the complete statistics of their lifetimes).

Despite the difficulties associated with the mathematical description of the two mechanisms (CLF and CR), numerous extensions and refinements of the original model have been considered.[20–27] For example, to account for CLF effects, a number of investigators have proposed to use a *position-dependent curvilinear diffusion coefficient* in the diffusion equation.[20–22] Others have added a *reaction-like term* to the diffusion equation with a position-dependent rate constant (following a similar approach to the same problem by Doi[3,14]).[23–25] CR, on the other hand, can also be taken into account by introducing a dynamic dilution parameter $\alpha$,[26,27] whereas a more sophisticated approach[17] makes use of a self-consistent methodology where the CR effect is calculated from the dynamics of tube constraints using information from the single-chain overall tube survival probability function, incorporating chain reptation and CLF effects. Inclusion of CLF and CR effects has led to tube models with an enhanced predictive capability as far as their agreement with experimental data (*e.g.*, for the shear moduli $G'(\omega)$ and $G''(\omega)$) is concerned. However, a molecular level understanding of the two mechanisms is still lacking. We mention, for example, that the entanglement time $\tau_e$ (the time at which a polymer chain starts to *feel* the tube constraint) for polybutadiene melts at 140 °C is computed from direct molecular simulations (based on the segmental mean square displacement) to be about 2–4 ns (see Table 2). If we make use of the value for the temperature shifting factor $a_T$ reported by Colby *et al.*,[28] which implies that $\tau_e = 4.4\text{–}6.5 \times 10^{-8}$ s at 25 °C, then we see that this is almost one order of magnitude smaller than the value ($\tau_e = 2.8\text{–}3.5 \times 10^{-7}$ s at 25 °C and 28 °C) employed by Pattamaprom *et al.*[24] in their model comparison against experimental data. On the other hand, there exists no experimental technique available today to directly probe PP dynamics at the molecular level and thus independently compute the values of the key variables and functions included in modern tube theories, such as the curvilinear diffusion coefficient $D_c(s,t)$ of the primitive chain segments and their survival probability function $\psi(s,t)$. To achieve this, it would be very helpful to deal with the problem from a different point of view, that of molecular simulations, and this is what we pursue in this work.

Molecular dynamics (MD) simulations allow one to observe how a molecular system evolves over time by accumulating the motion or trajectory of its state points through phase space by solving Hamilton's equations of motion.[29] They serve therefore as a bridge between the microscopic characteristics of the system and its macroscopic properties. Atomistic MD simulations have thus helped us elucidate structure–property relationships in polymeric systems under both equilibrium[30,31] and non-equilibrium conditions.[32,33] They are also useful in the development of coarse-grained (CG) models for polymers, in which a unit (usually termed as a bead or a super-atom) represents a collection of several atoms accounting effectively for an entire polymer segment.[34–43] It is a strategy that has been followed quite extensively in recent times to reduce computational cost in order to understand material behaviors over significantly longer time and

length scales. But one should be very careful with such an approach, since coarse graining at any level introduces irreversibility and additional dissipation in the system which, if forgotten or ignored, may severely limit the usefulness and range of applicability of the constructed model,[38] especially under non-equilibrium conditions.[44]

Although one can envisage a number of different coarse-grained models for polymers to describe the dynamics at the level of entire chains, one should keep in mind that (as already discussed above) the behavior of the system is governed by the existence of entanglements. Any meaningful coarse-grained model for polymers should therefore respect not only chain continuity but also chain uncrossability for the proper description of chain dynamics. The concept of topological constraints is central here since it helps describe the dynamics in the system in terms of the diffusive motion of the corresponding ensemble of primitive chains which is constrained within a cylindrical tube-like region of diameter $d_t$. The corresponding mathematical problem of the reduction from the trajectory of atomistic coordinates to the trajectory of primitive paths, has been addressed by Everaers *et al.*,[45] Kröger and co-workers,[46,47] and Tzoumanekas and Theodorou.[48] In a more recent study, Stephanou *et al.*[49] have proposed a methodology capable of quantifying chain dynamics in an entangled polymer melt *directly* in terms of the segment survival probability function $\psi(s,t)$ and its average $\Psi(t)$. The main advantage of the new methodology is that it automatically accounts not only for reptation but also for CLF and CR effects (and any other relaxation mechanisms present in the real system), since dynamics at the level of PPs is obtained by directly projecting data from a finer (atomistic-level) model. As such, the results obtained from this are ideal for a direct comparison with the predictions of modern tube models incorporating terms accounting for CLF and CR effects. Readers interested in methodological details are referred to the original publications,[49,50] where preliminary results from application of the technique to a number of model, moderately entangled linear polyethylene (PE) and *cis*- and *trans*-1,4-polybutadiene (PB) melts have been provided. Here we present additional results from simulations with polymer melts characterized by approximately 3–6 entanglements per chain, referring to the probability functions $\psi(s,t)$ and $\Psi(t)$ and their comparison with theoretically predicted curves. As we mentioned above, this type of information is not experimentally obtainable today, and this demonstrates the power and usefulness of the new methodology. On the one hand, it provides predictions for the linear viscoelastic properties of entangled melts, which can serve as an objective test for the assumed relaxation mechanisms and their mathematical description in theoretical approaches. On the other hand, it is very important to advance experimental techniques to directly obtain such microscopic information as $\psi(s,t)$ and $\Psi(t)$, which can be used for cross-checking as well as for exchanging information between computational, theoretical and experimental methods. It is only through this mutual complementary interaction between the three approaches that we can conceive a unified viewpoint for a variety of intricate phenomena occurring in polymeric materials without introducing unnecessary empiricism or assumptions.

The paper is organized in three sections as follows: in section 2 we give a brief account of the computational methodology and the simulated polymeric systems. In section 3, we present results of our PP analysis and compare them to several tube models. And in section 4 we summarize by discussing the major findings of the work and possible extensions.

## 2. Methodology and systems studied

Our computational methodology for calculating the function $\psi(s,t)$, which has been described in detail in a recent article,[49] includes the following steps:

(i) First, we determine the effective tube diameter $d_t$ either by analyzing the segmental mean square displacement (msd) $\phi(t) = \langle(\mathbf{r}_n(t) - \mathbf{r}_n(0))^2\rangle$ ($\mathbf{r}_n$ denotes the position vector of the $n^{\text{th}}$ atom along the chain) as a function of time [Fig. 1(a)] or by monitoring the displacement $N(t)$ of primitive chain segments (obtained by using the Z1-code[46,47]) orthogonal to the initial PP [Fig. 1(b)]. The average of the two values (which are practically the same) is then calculated and used in the subsequent PP analysis. We also determine the entanglement time $\tau_e$ and the disentanglement time $\tau_d$ by analyzing the segmental msd [see Fig. 1(a)] in the spirit of the reptation theory to identify the three characteristic breaks reflecting: the onset of tube constraints on segmental diffusion, the Rouse-like diffusion of atomistic units combined with tube constraints, and the crossover (at significantly longer times) to reptation dynamics.[3]

(ii) Given the estimated value of the tube diameter $d_t$ and the mapped trajectory of primitive chains (obtained by reducing the ensemble of atomistic configurations accumulated in the course of the MD simulations to an ensemble of primitive paths), we proceed to construct the initial (corresponding to time $t = 0$) curvilinear tube around each entanglement strand in a primitive chain. This is done geometrically by visiting entanglement strands (straight line segments) one after the other along the chain starting from either end and building the tube around them piece-by-piece in the form of a small cylinder whose axis coincides with the entanglement strand and whose diameter is equal to $d_t$. Entanglement strands meet at kink points, thus in the construction process some care should be taken to smooth out intersecting cylindrical volumes there to ensure that an overall uniform tube is obtained.

(iii) We place segments along the primitive chain at equidistant points in the normalized [0,1] interval by converting from variable $s$ to variable $s/L$ in order to monitor chain motion in and out of the tube at different points along its contour. A typical number is 101 points (including the two chain ends) implying that the interval between any two neighboring segments is 0.01. The true coordinate of each segment in the dimensional interval $[0,L]$ is always easily recovered (even if the segment has migrated to a new entanglement strand) by storing and continually keeping the instantaneous value of the contour length $L$ of the chain. The main task of step (iii) is then to record the displacement of each segment $s$ at all later times $t$ relative to its position at $t = 0$ and determine whether it has escaped the initial tube after a time $t$ or not, by measuring its shortest distance $x$ from the initial PP (refer to Fig. 2 in Ref. 49 for a schematic visualization of the concept).

(iv) As segments can escape from the tube either perpendicularly or longitudinally along the chain contour, the following two criteria are set: (i) if $x(s) > d_t/2$, the segment $s$ is assumed to have escaped the initial tube; (ii) if $x(s) \leq d_t/2$, the segment $s$ is

 

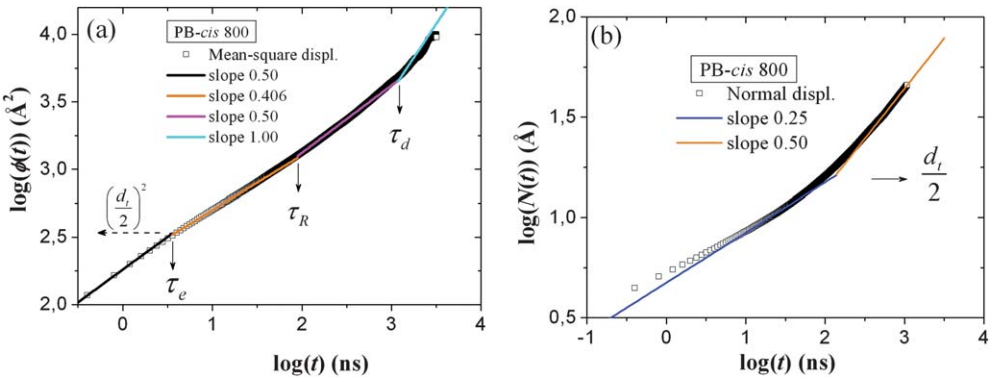


**Fig. 1** An illustration of the proposed two methodologies for estimating the tube diameter $d_t$ (the results refer to the PB-*cis* 800 system): (a) by plotting the mean-square displacement (msd) $\phi(t) = \langle(\mathbf{r}_n(t) - \mathbf{r}_n(0))^2\rangle$ of the innermost atomistic units *versus* time $t$ in a log–log plot to identify the four characteristic diffusive regimes indicative of reptation dynamics;[2] the tube diameter is then estimated as $d_t = 2\sqrt{\phi(t^*)}$ where $\phi(t^*)$ is registered at the time $t = t^*$ when the atomistic units start to feel the tube constraints which causes a change in the slope of the $\phi(t)$ *vs.* $t$ curve from 1/2 to 1/4[49] and (b) by observing the displacement $N(t)$ of the PP segments orthogonal to the initial primitive path (*i.e.*, the PP at time $t = 0$) *versus* time $t$ to check when the PP segments feel the tube constraint. This causes a break in the slope of the corresponding curve, which we find by fitting the curve before and after it with straight lines. The value of $N(t)$ at the intersection of the two lines provides an estimate of the tube radius $d_t/2$.[49]



assumed not to have escaped the tube perpendicularly but we should further check if it has escaped the tube longitudinally. If the segment $s$ has escaped the tube, then $\psi(s,t) = 0$; otherwise, $\psi(s,t) = 1$. In practice, there is always the possibility a chain segment, which at some time was found to be away from the initial tube, to return back to the tube at a later time (just as it diffuses around in space *via* thermal motion). To cover this case, a third criterion is set, called criterion of *permanent escape*; this tells us when a segment $s$ has *definitely* escaped the tube to completely erase its memory of the initial tube constraint. To formulate it we have been guided by Doi[51] who proposed a formula for computing fluctuations in the radius of the effective curvilinear tube as follows. Let $Q(r;\sigma)dr$ denote the probability that the nearest segments of the other chains lie at a distance $r$ within $dr$ from the given chain. This is a function of the dimensionless quantity $\sigma = (\langle R^2\rangle/6)^{1/2}/l$, where $\mathbf{R}$ denotes the chain end-to-end vector while $l$ is a measure of the intermolecular separation between chains; typically, $l = c^{-1/3}$ where $c$ denotes the chain number density. According to Doi,[51] one can get an estimate of the mean value of the tube radius by computing the average of the function $Q(r;\sigma)$, *i.e.*, by using $d_t/2 = \langle r\rangle = \int_0^\infty dr Q(r;\sigma) r$. Extending the argument to higher moments, we can therefore estimate the fluctuation in the tube radius by taking it to be equal to the second moment of $Q(r;\sigma)$, *i.e.*, as $\langle \Delta r^2\rangle^{1/2}$. We applied Doi's idea to all polymer melts simulated here and we found that to a good degree, $\langle \Delta r^2\rangle^{1/2} \approx d_t/2$, that is, the fluctuation in the tube radius is approximately equal to its average value. Our criterion for permanent escape is, therefore, formulated as follows: if the perpendicular displacement $x(s)$ of a segment $s$ at time $t$ is larger than the tube radius $d_t/2$ *and* smaller than the tube diameter $d_t$ (*i.e.*, if $d_t/2 < x(s) < d_t$), then $\psi(s,t) = 0$ as above *but* we allow the segment $s$ to return back to the original tube at later times due to thermal motion. This refers mostly to segments wiggling around in the vicinity of the outer surface of the tube, and it implies that these segments still keep the memory of the initial tube constraints. On the other hand, if the total perpendicular displacement of the segment is greater than the tube diameter (*i.e.*, if $x(s) > d_t$), then this segment is taken to have *completely* escaped the tube. That is, we put $\psi(s,t) = 0$ not only for the current time $t$ but also for *all subsequent times*, implying that such a segment has totally lost the memory of the initial tube (see Fig. 4 in Ref. 49 for a numerical example). From a mechanical point of view, this is equivalent to considering that such a segment (which has moved normally away from the tube a distance larger than its diameter) has been totally liberated by the initial topological constraints (thus also from the mechanical stress arising from them). Clearly, perpendicular escape is intimately related to the life time of entanglements. From a theoretical point of view, it reflects the release of local constraints, the mechanism known as constraint release (CR) as discussed in the Introduction; and it should be particularly important for weakly or moderately entangled polymers (such as the model melts studied in this work) or for bidisperse polymeric systems (mixtures of long and short chains of the same polymer).[52]

(v) For each PP segment $s$, the survival probability function $\psi(s,t)$ at any time $t$ is computed as the average value of all the zeros and all the ones recorded for this segment along all chains present in the system and for all possible time origins in the accumulated trajectory. Considering that homopolymer chains possess head-to-tail symmetry, the statistics can be improved even further by taking that $\psi(s,t) = \psi(1 - s,t)$.

A novel aspect of our approach is that it directly accounts for all CLF and CR effects, since the dynamical behavior of the system at the level of primitive paths is obtained by tracing first its microscopic dynamics (by solving Newton's equations of motion in the course of long MD simulations) and then reducing each of the accumulated melt configurations to a representation in terms of shortest paths for the chains that have the same topology with them and in addition they respect the underlying entanglement network as imposed by the condition of chain uncrossability. In fact, our methodology accounts not only for these effects (CLF and CR) but also for any other mechanism

present in the real polymeric system as long as this refers to length scales above the average step length of the primitive paths. Fingerprints of all these relaxation mechanisms are discernible at the level of the PP representation, since there is practically no loss of information in the projection from one level to the other (except for the dynamics at distances shorter than the Kuhn or step length of the PP). This is, indeed, an important feature of the approach. The methodology is also applicable to a number of polymeric systems of industrial relevance since it is independent of details related to the molecular architecture or composition of the constituent chains. Thus, it can deal with both homopolymer and block-copolymer melts, with both mono- and polydisperse samples, with bulk and interfacial systems, and with many others.

An interesting consequence of this work is that one can make use of the computed results for the $\psi(s,t)$ function and its average, $\Psi(t) = \int_0^1 \psi(s,t)ds$, to get estimates (in the framework of the tube theory) of the linear viscoelastic properties of the system. These include among others: (a) the relaxation modulus $G(t) = G_N^0\Psi(t)$ where $G_N^0$ is the plateau modulus, (b) the storage and loss moduli $G'(\omega) = G_N^0\omega\int_0^\infty \Psi(t)\sin(\omega t)dt$ and $G''(\omega) = G_N^0\omega\int_0^\infty \Psi(t)\cos(\omega t)dt$, respectively, (c) the zero-shear viscosity $\eta_0 = G_N^0\int_0^\infty \Psi(t)dt$, and (d) the steady-state shear compliance $J_e^0 = G_N^0\int_0^\infty t\Psi(t)dt/(G_N^0\int_0^\infty \Psi(t)dt)^2$.

The above methodology has been applied to a number of model linear polyethylene (PE) and *cis*-1,4- and *trans*-1,4-polybutadiene (PB) melts with a variety of chain lengths: $C_{320}$, $C_{400}$, and $C_{500}$ for the PE (denoted as PE320, PE400, and PE500, respectively), $C_{320}$, $C_{400}$, $C_{600}$, and $C_{800}$ for the *cis*-1,4-PB (denoted as PB-*cis*320, PB-*cis*400, PB-*cis*600, and PB-*cis*800, respectively) and $C_{320}$, $C_{400}$, and $C_{600}$ for the *trans*-1,4-PB ones (denoted as PB-*trans*320, PB-*trans*400, and PB-*trans*600, respectively).[31,49,53] All these melts are monodisperse except for the PB-*cis*320 and PB-*cis*400 ones which are characterized by a polydispersity index ($I$) slightly larger than one (as equal to $I =$ 1.08 and $I = 1.05$, respectively). The atomistic trajectories have been obtained by running isothermal–isobaric ($NPT$) MD simulations with a multiple time step algorithm at temperature $T = 450$ K and pressure $P = 1$ atm for the PE melts, and at temperature $T = 413$ K and pressure $P = 1$ atm for the PB melts. Sufficiently long trajectories (*e.g.*, from 750 ns for the PB-*cis*320 up to 4 μs for the PB-*trans*600 system in real time) were accumulated in all cases to reduce the statistical uncertainty of the computed statistical averages for the physical properties of interest and also to be able to trace dynamics up to times longer than the chain disentanglement time $\tau_d$ in each system. (Readers interested in further details of the employed MD method are referred to the ESI accompanying the present article.†).

The contour length reduction process to generate the network of PPs for a given atomistic configuration has been conducted *via* the Z1-code:[46,47] the chain ends of all chains are held fixed in space, the intramolecular excluded volume interactions are switched-off while maintaining the uncrossability conditions between different chains, and a set of geometric operations are employed that reduce the contour lengths of all polymer chains in the system to their minimum value simultaneously. After the minimization process has converged, the Z1-code produces a PP network corresponding to the ensemble of atomistic chains with a PP for each chain in the system; the PP contour length $L$ for each chain can thus be directly obtained by measuring the distance from one chain end to the other along the PP. In addition to this, the Z1-code provides the positions of the interior "kinks"[46,47] along the PP for each chain. We mention here that the Z1-code bears several similarities with the so-called CReTA algorithm proposed by Tzoumanekas and Theodorou.[48] Therefore, the main conclusions drawn from this work should not be considered as being specific to the application of the Z1-code but rather being representative of a more general class of this type of numerical codes that employ geometric operations on an ensemble of atomistic chains to attain the entanglement network of PPs.

## 3. Results and discussion

In Table 1, we present the simulation results for the density $\rho$, the mean square chain end-to-end distance $\langle R^2\rangle$, and the average

**Table 1** Numerical results for the density $\rho$, the mean square chain end-to-end distance $\langle R^2\rangle$, the average PP contour length $\langle L\rangle$, the packing length $p$, and the step length $a_s$ of the PP for the simulated melts at temperature $T = 450$ K for the PE melts and $T = 413$ K for the PB melts (in all cases, the pressure $P$ was set equal to 1 atm)

| System[a] | $\rho$/g cm$^{-3}$ | $\langle R^2\rangle$/Å$^2$[b] | $\langle L\rangle$/Å[c] | $p$/Å[d] | $a_s$/Å[e] |
|---|---|---|---|---|---|
| PE320 (32) | 0.767 | 6060 ± 150 (8.0) | 162 ± 4 (0.33) | 1.60 | 37.4 ± 2.2 |
| PE400 (16) | 0.768 | 7675 ± 287 (8.1) | 198 ± 6 (0.32) | 1.58 | 38.7 ± 3.3 |
| PE500 (16) | 0.769 | 10679 ± 472 (9.0) | 251 ± 8 (0.33) | 1.42 | 42.5 ± 4.7 |
| PB-*trans*320 (32) | 0.837 | 4076 ± 130 (5.9) | 104 ± 4 (0.22) | 1.58 | 38.9 ± 2.6 |
| PB-*trans*400 (32) | 0.838 | 4865 ± 139 (5.6) | 127 ± 5 (0.22) | 2.10 | 38.1 ± 2.3 |
| PB-*trans*600 (32) | 0.838 | 7233 ±181 (5.6) | 185 ± 5 (0.21) | 2.20 | 39.1 ± 2.4 |
| PB-*cis*320 (32) | 0.863 | 3280 ± 102 (4.8) | 86 ± 4 (0.18) | 2.22 | 38.0 ± 2.5 |
| PB-*cis*400 (32) | 0.865 | 4035 ± 102 (4.7) | 104 ± 4 (0.18) | 2.54 | 38.6 ± 2.1 |
| PB-*cis*600 (32) | 0.864 | 6381 ± 160 (4.9) | 154 ± 6 (0.17) | 2.57 | 41.5 ± 2.5 |
| PB-*cis*800 (24) | 0.864 | 8791 ± 221 (5.1) | 202 ± 9 (0.17) | 2.44 | 43.4 ± 2.5 |

[a] The numbers in parentheses indicate the number of chains in the system. [b] The numbers in parentheses represent the characteristic ratio $C_n \equiv \langle R^2\rangle/(N-1)\bar{l}^2$ where $N$ is the average number of carbon atoms per chain and $\bar{l}$ the average bond length (as equal to 1.54 Å and 1.47 Å for the PE and PB melts, respectively). [c] The number in parentheses represent the effective PP length per atomic bond, as equal to $L/(N-1)\bar{l}$. [d] The packing length $p$ is calculated as $p = M/(\rho N_A\langle R^2\rangle)$ where $M$ is the molecular weight of polymer and $N_A$ is Avogadro's number. [e] The PP step length $a_s$ estimated by $a_s = \langle R^2\rangle/\langle L\rangle$ for the simulated polymer melts.

 

value $\langle L \rangle$ of the PP contour length, for all the polymer systems studied in the course of this work (PE, *cis*-1,4-PB and *trans*-1,4-PB). Focusing on the density data first, we notice the following: a) the reported values are independent of the molecular weight (MW) of the simulated samples (as observed experimentally for polymers with MW above a certain value, *e.g.*, the chain length $N \approx 250$ observed from the previous simulations[31,47]), b) PE melts are characterized by a lower density than *cis*-1,4 and *trans*-1,4-PB ones (this is partly due to the higher temperature at which PE was simulated here), and c) *cis*-1,4-PB has a slightly higher density than *trans*-1,4-PB at the same temperature. All of the above results are consistent with published experimentally measured data for the three polymers.[54] Regarding the average chain dimensions, the data in Table 1 indicate that for the same number of carbon atoms per chain, PE chains are significantly longer than *trans*-1,4-PB chains (by approximately 50%), which, in turn, are longer than their corresponding *cis*-1,4-PB analogues (by approximately 15%). The fact that PE is characterized by a larger chain end-to-end distance than PB indicates that it has a higher stiffness. The *cis*-1,4-PB chain, on the other hand, is shorter than the corresponding *trans*-1,4-PB one, which reflects the more compact arrangement of the four carbon atoms on the two sides of the double bond in the corresponding monomeric unit (*trans* torsional states always lead to more extended conformations than *cis* ones). All these conclusions are reflected on the values of the characteristic ratio $C_N$ for the three polymers, defined as $C_N \equiv \langle R^2 \rangle / (N-1)\bar{l}^2$ where $N$ denotes the average number of carbon atoms per chain and $\bar{l}$ the average length per bond (this is equal to 1.54 Å for a PE molecule and equal to 1.47 Å for a PB molecule). The simulation data for $C_N$ (as reported in the third column of Table 1 under the results for $\langle R^2 \rangle$) are seen to be in general agreement with experimental data according to which, in the limit of infinitely long chains, $C_N$ tends to $7.8 \pm 0.3$ for PE,[55,56] to $4.9 \pm 0.2$ for *cis*-PB and to $5.8 \pm 0.2$ for *trans*-PB.[57] Regarding the variation of $\langle L \rangle$ with chain length, for all practical purposes this is found to be linear for the three polymers which is in agreement with the basic concepts of the reptation theory.[2,3] Overall, for the same number of carbon atoms per chain, the PE melts are characterized by larger $\langle L \rangle$ values than PB melts. *Trans*-PB melts, on the other hand, exhibit $\langle L \rangle$ values that are larger than those of the corresponding *cis*-PB analogues (melts of the same length), a direct consequence of their more extended conformation. A better measure of the PP contour length is provided by the dimensionless parameter $L/(N-1)\bar{l}$ expressing the effective PP length stored per atomic bond. Its value for the three types of polymers studied here is also reported in Table 1 ($\sim$0.33 for PE, $\sim$0.22 for *trans*-PB, and $\sim$0.17 for *cis*-PB) indicating differences which are consistent with the corresponding $\langle R^2 \rangle$ data.

Two very important parameters reported in Table 1 are: (a) the packing length $p = M/(\rho N_A \langle R^2 \rangle)$, and (b) the step length $a_s = \langle R^2 \rangle / \langle L \rangle$ of the primitive path, where $M$ denotes the molecular weight of the polymer and $N_A$ the Avogadro number. Their values are related to the degree of chain entanglement and mesh size of the underlying topological network, respectively, in the polymer. The packing length $p$, in particular, is used quite extensively in the polymer literature to relate rheological properties with chain dimension, since it embodies information about both chain conformation and monomer packing.[54,58–61] The simulation results are in favour of a smaller $p$ value for PE compared to PB, and this should be interpreted as an indication that PE chains overlap more than PB chains. In turn, this implies that topological interactions in PE are stronger than in PB, which should be associated with the more compact structure of the PB chains. Comparing the computed $p$ values for the two PB polyisomers, on the other hand, leads us to the conclusion that *cis*-PB chains experience weaker topological interactions than *trans*-PB chains. As far as the average value of the step length $a_s$ of the PP in the three polymers is concerned, our simulation results indicate the following order: $a_s$(*cis*-PB melt) > $a_s$(*trans*-PB melt) > $a_s$(PE melt), which is the opposite to that observed for the packing length $p$. [Here we note that as the two shortest PB-*cis* systems (PB-*cis*320 and PB-*cis*400) are only slightly entangled (*i.e.*, $Z \sim 2$) and thus lie in the transition zone between the Rouse and reptation regimes, their results for $a_s$ are considered to be less meaningful than those of the more entangled (longer) systems from the standpoint of the reptation theory which becomes more accurate for more entangled systems. In addition, the relatively large value of $a_s$ computed for the PE500 melt manifests in all probability finite system size effects due to the rather small number of chains, only sixteen, employed in the MD simulations with this system.]

In Table 2 we report the results of our computational approach for the entanglement time $\tau_e$, the disentanglement time $\tau_d$, and the tube diameter $d_t$, for the simulated PE and PB melts. The first thing to notice in the data of the Table is that $d_t$ and $\tau_e$ are practically chain-length independent even for the moderately entangled polymer melts addressed here, which agrees with the basic notion of the reptation theory that the time it takes a chain segment to "hit" the tube (and thus feel the topological constraints imposed by the presence of the other chains) and the average diameter of the effective tube (providing a measure for these topological interactions) is independent of chain length. More precisely, $\tau_e$ comes out to be roughly between 2–4 ns while

**Table 2** Results for the tube model parameters of the simulated systems (entanglement time $\tau_e$, disentanglement time $\tau_d$, and the tube diameter $d_t$), as obtained from the methods described in the text based on the segmental msd data

| System | $\tau_e$/ns | $\tau_d$/ns | $d_t$/Å[a] |
|---|---|---|---|
| PE320 | $2.1 \pm 0.5$ | $316 \pm 32$ | $32.8 \pm 2.0$ |
| PE400 | $2.9 \pm 0.4$ | $489 \pm 25$ | $32.9 \pm 2.8$ |
| PE500 | $2.8 \pm 0.4$ | $1042 \pm 46$ | $32.4 \pm 2.5$ |
| PB-*trans*320 | $3.2 \pm 0.7$ | $264 \pm 34$ | $25.9 \pm 2.7$ |
| PB-*trans*400 | $3.1 \pm 0.5$ | $355 \pm 25$ | $26.0 \pm 2.3$ |
| PB-*trans*600 | $3.2 \pm 0.5$ | $1204 \pm 50$ | $28.9 \pm 2.9$ |
| PB-*cis*320 | $1.8 \pm 0.4$ | $138 \pm 18$ | $31.5 \pm 2.1$ |
| PB-*cis*400 | $2.3 \pm 1.0$ | $256 \pm 24$ | $29.1 \pm 1.7$ |
| PB-*cis*600 | $2.1 \pm 0.8$ | $500 \pm 70$ | $29.9 \pm 1.5$ |
| PB-*cis*800 | $2.3 \pm 0.5$ | $1255 \pm 80$ | $30.3 \pm 1.6$ |

[a] The tube diameter is calculated here as

$$d_t = 2\sqrt{\phi(t^*)}$$

where $\phi(t^*)$ denotes the segmental msd at the time $t = t^*$ where the slope of $\phi(t)$ starts to deviate from ½ as segments leave the initial $t^{1/2}$-regime (in a log–log plot) and enter the following $t^{1/4}$-regime [Fig. 1(a)].[49] The results are found to be quantitatively similar to those obtained by monitoring the perpendicular displacement of the PP segments at the time marking the onset of tube constraints on their motion [Fig. 1(b)].

$d_t$ assumes values in the range of 26–33 Å for the three polymers. Furthermore, by comparing the simulation data for the average tube diameter $d_t$ reported in Table 2 and the average PP step length $a_s$ reported in Table 1 we see that their values are not the same, as $a_s$ comes out to be larger than $d_t$ by 15–40%. This is a significant finding from the present analysis: the relation between $d_t$ and $a_s$ is not clear in the tube theory and the two concepts are used interchangeably in the tube models (or, better, they are considered as different quantities but with the understanding that their values are practically the same). An effort to define a quantitative relationship between $d_t$ and $a_s$ was made by Öttinger[62] on the basis of the Porod–Kratky model for polymer chains coarse-grained to the level of smooth primitive paths by assuming the action of two competing springs along the lateral and longitudinal directions of the chain's main contour (accounting for the competition between chain connectivity and chain uncrossability). Öttinger[62] found that $a_s$ is equal to $2d_t$ for this model, which is in qualitative agreement with the results of our direct PP analysis.

As already alluded to above, CLFs are important for most polymers in practical applications. Both statistical–mechanical and analytical theories[3,14] suggest that $\Delta L/\langle L\rangle$ decreases with chain length as $\Delta L/\langle L\rangle = XZ^{-1/2}$ where $X$ is a numerical constant and $Z$ the (average) number of entanglements per chain. Based on a variational calculation, Doi[14] has argued that the value of $X$ should be larger than 1.47. des Cloizeaux[63] and Needs,[64] on the other hand, have proposed that $X$ should be significantly smaller than 1.47, approximately equal to 0.7 and 0.3, respectively. By treating CLF as a non-Markovian stochastic process, Ketzmerick and Öttinger[65] seem to favor Doi's value ($X = 1.47$). A different scaling is supported by the slip-link numerical simulations of Masubuchi *et al.*,[42] according to which $\Delta L/\langle L\rangle$ should vary with $Z$ (not as $\Delta L/\langle L\rangle = XZ^{-1/2}$ but) as $\Delta L/\langle L\rangle = YZ^{-1}$ with $Y = 3$. To shed some more light on the issue, in Fig. 2 we plot $1 - \Delta L/\langle L\rangle$ *versus* $Z$ for all polymer melts simulated here. The results have been obtained by using a value for the entanglement length $N_e$ (as estimated by $N_e = N\langle R^2\rangle/\langle L\rangle^2$) equal to 75 ± 11 for all PE systems, equal to 119 ± 15 for all *trans*-PB systems, and equal to 144 ± 19 for all *cis*-PB systems.[49] Our curves seem to favor Doi's original suggestion that $\Delta L/\langle L\rangle = XZ^{-1/2}$ but with $0.5 \le X \le 0.7$ as proposed by des Cloizeaux[63] and Needs.[64] In fact, if we neglect the data for the two shortest computational samples (PB-*cis*320 and PB-*cis*400), the optimal value for $X$ comes out to be approximately 0.5, but clearly more MD data are needed (preferably for longer chain samples and for polymers other than linear PE and PB) to make a more conclusive statement. In the same graph, we have also plotted the curve corresponding to the scaling law suggested by the slip-link simulations of Masubuchi *et al.*[42] (that $\Delta L/\langle L\rangle = 3Z^{-1}$); it is clear that (at least for the moderately entangled polymers addressed here) their model overestimates the CLF effect. We close our discussion here by mentioning that: (a) the predicted value of $X$ from the PP analysis is close to the value of $X = 3^{-1/2} \approx 0.58$ obtained by assuming a Gaussian distribution for contour lengths around $\langle L\rangle$,[3,14,66] and (b) Liu *et al.*[67] have proposed that the value $X = 0.7$ for CLF effects is consistent with experimental data.

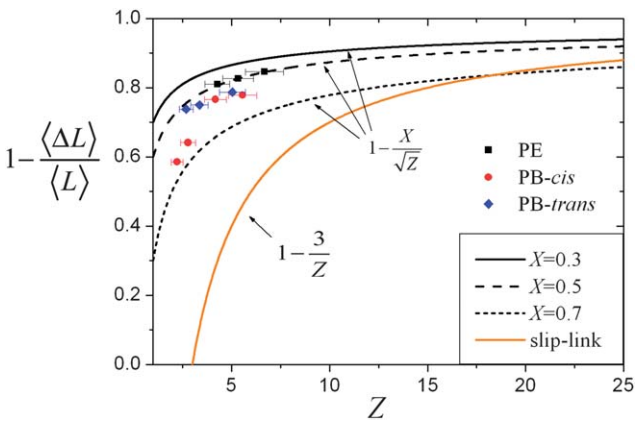


**Fig. 2** A plot of the average fluctuation $1 - \langle\Delta L\rangle/\langle L\rangle$ of the PP contour length where $\langle\Delta L\rangle \equiv (\langle L^2\rangle - \langle L\rangle^2)^{1/2}$ with the number of entanglements $Z$ per chain for all simulated systems. The results are compared with Doi's theoretical prediction (Ref. 14) that $1 - \langle\Delta L\rangle/\langle L\rangle = 1 - X/\sqrt{Z}$ for different values of the numerical coefficient $X$. If we ignore the two shortest *cis*-PB melts, the best fits to the simulation curves are obtained for $X \approx 0.5$. Also included in the figure is the curve corresponding to the scaling $1 - \langle\Delta L\rangle/\langle L\rangle = 1 - 3/Z$ reported by Masubushi *et al.* on the basis of slip-link simulations.[42]

A quantity directly related to CLFs is the rate of decay of the time auto-correlation function for the contour length $L$. By considering PP segments along the chain contour to follow a one-dimensional Rouse motion, Doi showed that:[3,14]

$$\frac{\langle L(t)L(0)\rangle - \langle L(t)\rangle^2}{\langle L^2(t)\rangle - \langle L(t)\rangle^2} = \sum_{p:\text{odd}}^{\infty} \frac{8}{(p\pi)^2} \exp\left(-\frac{p^2 t}{\tau_R}\right) \qquad (1)$$

where $\tau_R$ is the Rouse time of the chain. We provide a test of eqn (1) in Fig. 3 where we show plots of the normalized time auto-correlation function of the contour length for the PE400, PB-*cis*600, and PB-*trans*600 melts as extracted from our topological analysis. As can be directly seen from the fits to the data in the figure, the weighted sum of simple exponential functions in eqn (1) (represented by dashed lines in Fig. 3) does not provide a satisfactory description of the simulation data. A better overall fit to the data is obtained by a stretched exponential or KWW (Kohlrausch–Williams–Watts) function (represented by solid lines in Fig. 3) of the form $A\exp[-(t/\tau_{KWW})^{\beta_{KWW}}]$ corresponding to a correlation time $\tau_c = A\frac{\tau_{KWW}}{\beta_{KWW}}\Gamma\left(\frac{1}{\beta_{KWW}}\right)$ where $\Gamma(.)$ denotes the Gamma function.[68] It is then of interest to check how the corresponding correlation (relaxation) time $\tau_c$ varies with chain length and from polymer to polymer, and how it compares to the corresponding Rouse time $\tau_R$. It turns out that $\tau_c$ is about 30–50% smaller than $\tau_R$ for all simulated PE and *cis*-PB systems, but almost two times larger than $\tau_R$ for all *trans*-PB melts. These results are useful on their own since they indicate that CLF effects may depend (at least as far as a quantitative description is concerned) on the molecular and architectural details of the polymer.

In Fig. 3 two additional functions are plotted: (a) the time auto-correlation function of the chain end-to-end unit vector $\langle\mathbf{R}(t)\cdot\mathbf{R}(0)\rangle/\langle R^2\rangle$ determined directly from the atomistic MD simulations, and (b) the overall survival probability $\Psi(t)$ obtained from the proposed computational analysis for relaxation at the level of PPs by integrating the function $\psi(s,t)$ over $s$. In

 

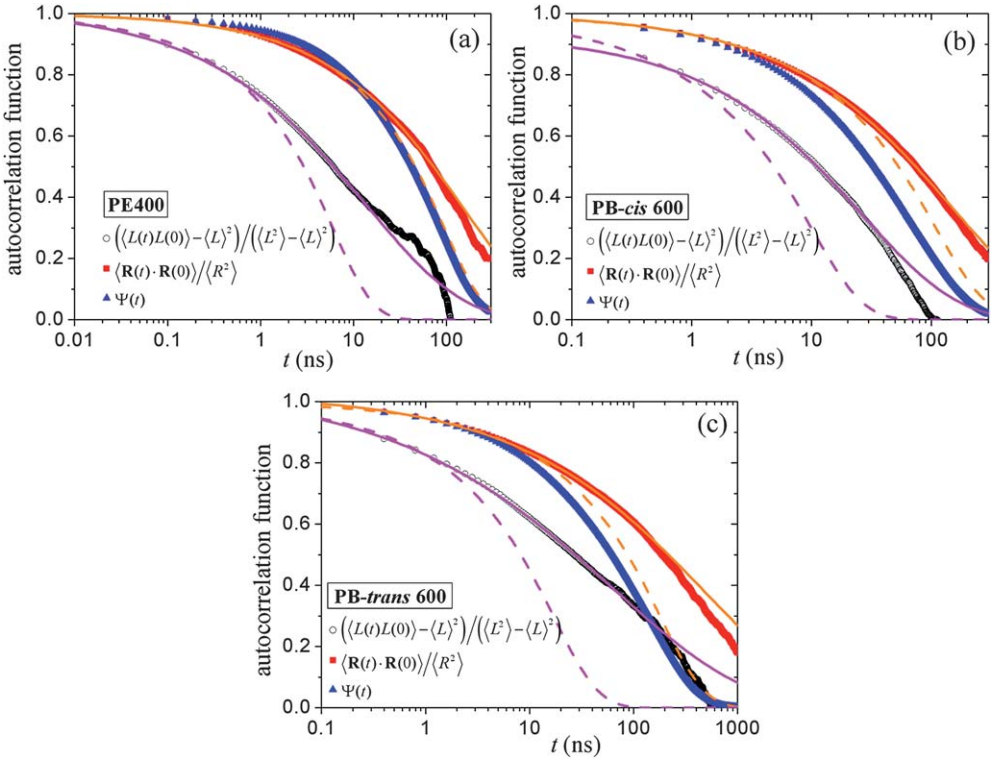


**Fig. 3** A comparison of the function $\Psi(t)$ determined from the proposed PP analysis for three of the simulated melts (PE-400, PB-*cis*600 and PB-*trans*600) with the time auto-correlation functions of the chain end-to-end vector $\langle \mathbf{R}(t)\cdot\mathbf{R}(0)\rangle/\langle R^2\rangle$ and of the PP contour length $(\langle L(t)L(0)\rangle - \langle L\rangle^2)/(\langle L^2\rangle - \langle L\rangle^2)$. The solid and dashed lines represent the best fits to the simulation data by a KWW stretched exponential function and the weighted sum of simple exponential functions [eqn (1) and (2)], respectively; orange lines refer to $\langle \mathbf{R}(t)\cdot\mathbf{R}(0)\rangle/\langle R^2\rangle$ and purple lines to $(\langle L(t)L(0)\rangle - \langle L\rangle^2)/(\langle L^2\rangle - \langle L\rangle^2)$.



the original Doi–Edwards model, $\langle \mathbf{R}(t)\cdot\mathbf{R}(0)\rangle/\langle R^2\rangle$ is given by the following equation:

$$\langle \mathbf{R}(t)\cdot\mathbf{R}(0)\rangle/\langle R^2\rangle = \sum_{p;\text{odd}}^{\infty} \frac{8}{(p\pi)^2}\exp\left(-\frac{p^2 t}{\tau_d}\right) \qquad (2)$$

The following two conclusions are drawn from the graphs of Fig. 3: (a) The relaxation of the chain unit end-to-end vector is significantly slower compared to that of the PP contour length; this is clearly consistent with the tube model which predicts that $\langle \mathbf{R}(t)\cdot\mathbf{R}(0)\rangle/\langle R^2\rangle$ should scale with the disentanglement time $\tau_d$ while $\dfrac{\langle L(t)L(0)\rangle - \langle L(t)\rangle^2}{\langle L^2(t)\rangle - \langle L(t)\rangle^2}$ should scale with the Rouse time $\tau_R$ of the chain. (b) In the original Doi–Edwards model where CR effects are neglected, the functions $\langle \mathbf{R}(t)\cdot\mathbf{R}(0)\rangle/\langle R^2\rangle$ and $\Psi(t)$ are equivalent: one can prove that one is equal to the other [see eqn (6.15) in Ref. 3]. In the presence of CR, however, which should be the case in the presently simulated melts, $\Psi(t)$ must drop faster than $\langle \mathbf{R}(t)\cdot\mathbf{R}(0)\rangle/\langle R^2\rangle$ since by locally releasing entanglements along the chain contour, such a mechanism should accelerate dynamics at the level of the (stress) function $\Psi(t)$ without affecting dynamics at the level of the end-to-end vector. The graphs depicted in Fig. 3 confirm this, since $\Psi(t)$ is seen to drop considerably faster than $\langle \mathbf{R}(t)\cdot\mathbf{R}(0)\rangle/\langle R^2\rangle$ for all simulated systems. In addition, it is seen again from the figure that the data is better fitted by a KWW function (represented by orange solid lines) than the weighted sum of simple exponential functions in eqn (2) (represented by orange dashed lines).

We now turn our attention to a key function in all tube models, the segment survival probability $\psi(s,t)$ expressing the probability that chain (or tube) segment $s$ remains after time $t$. Part (a) of Fig. 4 presents the computed $\psi(s,t)$ profiles for the simulated *cis*-PB melts as a function of normalized time (units of $\tau_d$) for all segments in the normalized interval [0,1]. The graphs for the different chain-length systems are considered to be consistent with each other (the little deviations observed for the PB-*cis*800 system are mainly attributed to the larger statistical error with which $\tau_d$ is computed for this system from the log–log msd plot of the corresponding atomistic segmental msd). At the very early times (*i.e.*, for $t/\tau_d = 0.01$ in Fig. 4(a) corresponding to $t \sim \tau_e$), the value of the function $\psi(s,t)$ for the majority of middle segments ($0.2 \leq s \leq 0.5$) is close to unity, indicating that these are still inside the initial tube. In turn, this suggests that chain reptation and CR effects are rather unimportant at these very early times. In contrast, for primitive chain segments closer to the two chain ends, $\psi(s,t)$ is significantly smaller than unity, indicating that these have started escaping the constraints of the original tube. This behaviour is fully consistent with the basic ideas of the reptation theory and the underlying tube model, and proves the significance of CLF effects especially for segments near the chain ends. In fact, our computations reveal that even for the two segments *exactly* at the two ends ($s = 0$ and $s = 1$), the function $\psi(s,t)$ remains above zero for some finite time. This observation, which has also been made in some previous simulations with a coarse-grained model for the polymer chains,[69,70] contradicts the customary assumption of the tube models (made partly for

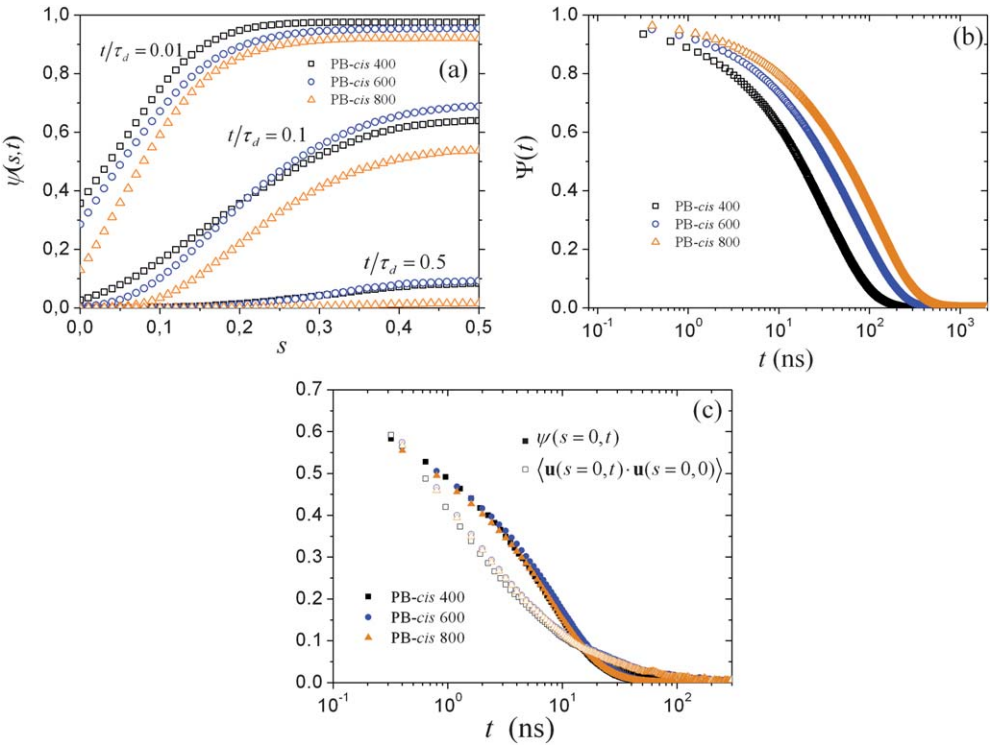


**Fig. 4** (a) Plots of the segment survival probability function $\psi(s,t)$ (describing the probability that a primitive chain segment $s$ remains in the initial tube after time $t$) at three different times (early, intermediate, and late), as obtained from the present PP analysis for the four simulated *cis*-PB melts. (b) Same as with (a) but for the average tube survival probability function $\Psi(t) \equiv \int_0^1 \psi(s,t)ds$ representing the fraction of the primitive chain that remains in the initial tube after time $t$. (c) End-segment relaxation based on the computed data for $\psi(s = 0,t)$ and $\psi(s = 1,t)$ (filled symbols) and on the time auto-correlation functions $\langle \mathbf{u}(s = 0,t)\cdot\mathbf{u}(s = 0,0)\rangle$ and $\langle \mathbf{u}(s = 1,t)\cdot\mathbf{u}(s = 1,0)\rangle$ of the corresponding tangent unit vectors $\mathbf{u}$ (empty symbols).

reasons of mathematical simplicity) that $\psi(s,t) = 0$ for $s = 0$ and $s = 1$ for all times $t > 0$. Even if the consequences of such an assumption are negligible for truly long polymers, they must be taken into account in the case of weakly entangled melts, in particular if one wishes to make a direct and quantitative comparison of the predictions of the model with measured data. By accounting, for example, for the non-zero life time of PP end segments, van Ruymbeke *et al.*[71] in a recent study managed to resolve the so-called "time–stress discrepancy" problem, namely the inability of tube models to describe the apparent plateau modulus of weakly-entangled, nearly monodisperse linear polymer melts, despite their capability to predict rather accurately the terminal relaxation times. The discrepancy was shown to be due to an overestimation of CLF for the outer molecular segments. By accounting, therefore, in their time marching algorithm for the fact that a chain needs a short (non-zero) time practically equal to the entanglement time $\tau_e$ (*i.e.*, as observed in our previous study[49] but also in the present computations) to be considered in equilibrium within its tube, van Ruymbeke *et al.*[71] resolved the discrepancy satisfactorily.

Also shown in Fig. 4(a) are profiles of the computed $\psi(s,t)$ curves at times longer than $\tau_e$ (comparable, for example, to $\tau_d$). Clearly, as time increases, the entire $\psi(s,t)$ curve falls to lower values, implying that more and more PP segments escape the initial tube due to reptation, CLF, and CR mechanisms. For the relatively short (moderately entangled) polymer systems, studied here, both mechanisms play a key role in the relaxation of chains in the melt.

In Fig. 4(b) we present our results for the overall survival probability $\Psi(t)$ (the average of $\psi(s,t)$ over $s$) for the simulated *cis*-1,4-PB systems, representing the average fraction of primitive chain segments remaining in the initial tube after time $t$. Clearly, longer chains relax slower than shorter ones, thus the computed $\Psi(t)$ curve for PB-*cis*800 lies always above that of PB-*cis*600 whose $\Psi(t)$ is, in turn, always above that of PB-*cis*400. We also observe that the $\Psi(t)$ curves cannot be accurately represented by the weighted superposition of simple exponentials as predicted by the original Doi–Edwards model;[2,3] instead, one should resort to a fitting with a stretched-exponential function, in which case

**Table 3** Values of the characteristic relaxation times ($\tau_c$) of the simulated systems as estimated by the integral of: (a) the stretched-exponential curve (*e.g.*, $A\exp[-(t/\tau_{KWW})^{\beta_{KWW}}]$) describing the decay of the overall survival probability function $\Psi(t)$, and (b) the segment survival probability $\psi(s,t)$ at the two chain ends ($s = 0$ or $s = 1$)

| System | $\Psi(t)$ | $\psi(s = 0,t)^a$ |
|---|---|---|
| PE400 | 75 ± 5 | 3.8 ± 0.7 (2.3 ± 0.3) |
| PE500 | 137 ± 9 | 4.7 ± 0.9 (2.3 ± 0.3) |
| PB-*trans*400 | 59 ± 5 | 4.8 ± 0.7 (7.2 ± 1.4) |
| PB-*trans*600 | 127 ± 7 | 5.4 ± 0.8 (6.9 ± 1.3) |
| PB-*cis*600 | 65 ± 8 | 4.5 ± 0.7 (6.5 ± 0.8) |
| PB-*cis*800 | 104 ± 11 | 5.1 ± 0.7 (7.4 ± 1.4) |

[a] The results denote the average of the $\psi(s,t)$ values for $s = 0$ and $s = 1$. Numbers in parentheses indicate relaxation times based on the decay of the time auto-correlation function $\langle \mathbf{u}(s = 0,t)\cdot\mathbf{u}(s = 0,0)\rangle$ of the unit vector $\mathbf{u}$ of the corresponding end-strands.

 

one obtains the correlation times that are reported in the second column of Table 3. Rather large differences between these times and the corresponding disentanglement times $\tau_d$ (reported in Table 2) are observed, which can be explained by the enhanced role of CLF and CR mechanisms (that are neglected in the original theory for reptation in a fixed network of obstacles), especially for the rather short polymers studied in the present work.

In Fig. 4(c) we show how $\psi(s,t)$ decreases with time at the two end segments ($s = 0$ and $s = 1$); we also show the decay of the corresponding time auto-correlation functions $\langle \mathbf{u}(s = 0,t)\cdot\mathbf{u}(s = 0,0)\rangle$ and $\langle \mathbf{u}(s = 1,t)\cdot\mathbf{u}(s = 1,0)\rangle$ for the tangent unit vectors $\mathbf{u}$ along the first and last entanglement strands in the chain (reporting always the average of the function values for $s = 0$ and $s = 1$). Despite that the two sets of curves do not superimpose, they indicate that end segment relaxation: (a) is independent of chain length (see also numerical data in Table 3), and (b) is brought to completion after a time approximately equal to $\tau_e$.[49]

Practically the same conclusions are drawn from the analysis of the accumulated PP data for the *trans*-PB and PE melts; the corresponding graphs for the functions of interest in this work ($\psi(s,t)$, $\Psi(t)$, $\psi(s = 0,t)$or $\psi(s = 1,t)$, and $\langle \mathbf{u}(s = 0,t)\cdot\mathbf{u}(s = 0,0)\rangle$ or $\langle \mathbf{u}(s = 1,t)\cdot\mathbf{u}(s = 1,0)\rangle$) are shown in Fig. 5 for the simulated *trans*-PB melts and in Fig. 5 of Ref. 49 for the simulated PE melts. Furthermore, in Fig. 6 we compare the results of our PP analysis for $\psi(s,t)$, $\Psi(t)$, and $\psi(s = 0,t)$ for three of the simulated systems (PE400, PB-*trans*600, and PB-*cis*800) which are characterized by practically the same (average) number of entanglements $Z = N/N_e$ per chain (5.33 ± 1.15, 5.04 ± 0.93, and 5.56 ± 1.07, respectively, as estimated from the $N_e$ values given above). Although the resulting curves do not superimpose, their shapes are quite similar, especially those between the *cis*- and *trans*-PB melts. This is quite interesting given that *cis*- and *trans*-PB systems are characterized by very different values of their segmental (or monomeric) friction coefficient $\zeta$: based on the chain center-of-mass diffusion coefficient,[31] $\zeta$ for *trans*-PB is reported equal to $7.2 \pm 0.5 \times 10^{-10}$ dyn s cm$^{-1}$ which is approximately twice as large as the value $3.2 \pm 0.2 \times 10^{-10}$ dyn s cm$^{-1}$ reported for *cis*-PB.[72] The large differences observed in the computed values of the function $\psi(s,t)$ between PB and PE melts having the same number of entanglements per chain (which are larger than the corresponding differences in the values of their segmental friction coefficients[30,31]) suggests that stress relaxation in a polymeric liquid is a rather complicated issue involving more factors than just $Z$ and $\zeta$. The same conclusion is drawn if we compare the $\Psi(t)$ and $\psi(s = 0,t)$ plots in the three systems (shown in parts (b) and (c), respectively, of Fig. 6).

We proceed now to a direct comparison of our computed results for the function $\psi(s,t)$ with the predictions of well known tube models. We have decided to limit the comparison to only the case of the PE500 melt, since this is the most entangled of all the presently simulated melts, characterized by an average number of entanglements per chain $Z = 6.67$. Furthermore, and since there have been many modifications of the tube model, the comparison refers only to those models for which the function $\psi(s,t)$ is either analytically known or numerically obtainable through the solution of a partial differential equation. The following three models have thus been considered: (a) the des Cloizeaux model,[73] (b) the Pattamaprom *et al.* model,[23] and (c) the Leygue *et al.*[21] model. For the purpose of the comparison with the pure reptation

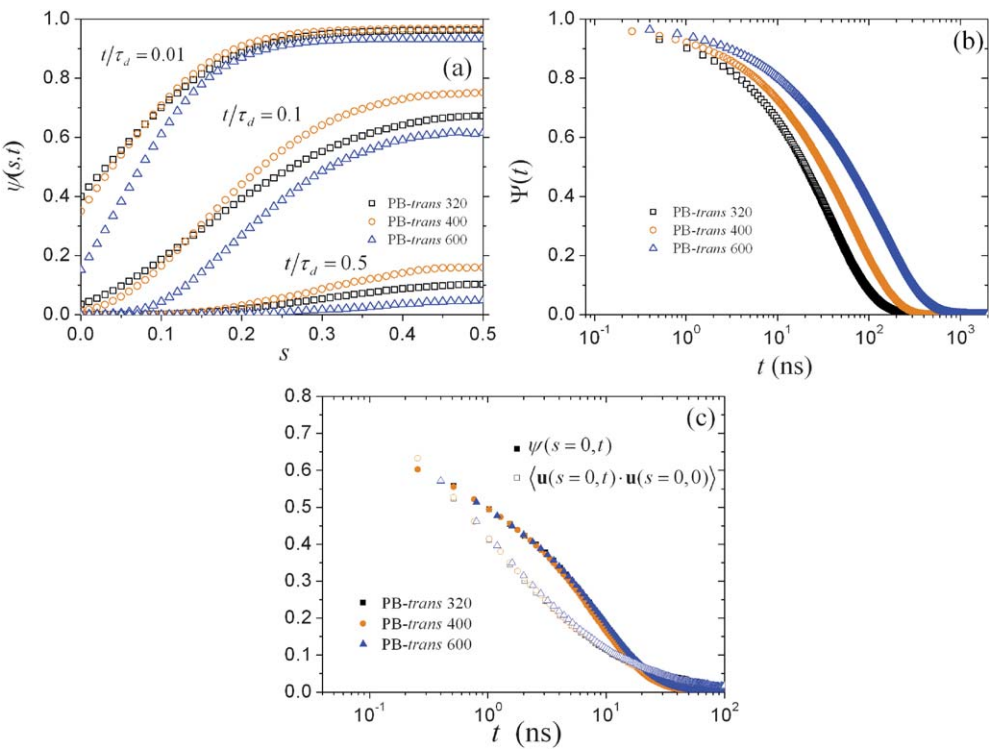


**Fig. 5** Same as with Fig. 4, but for the *trans*-PB melts.

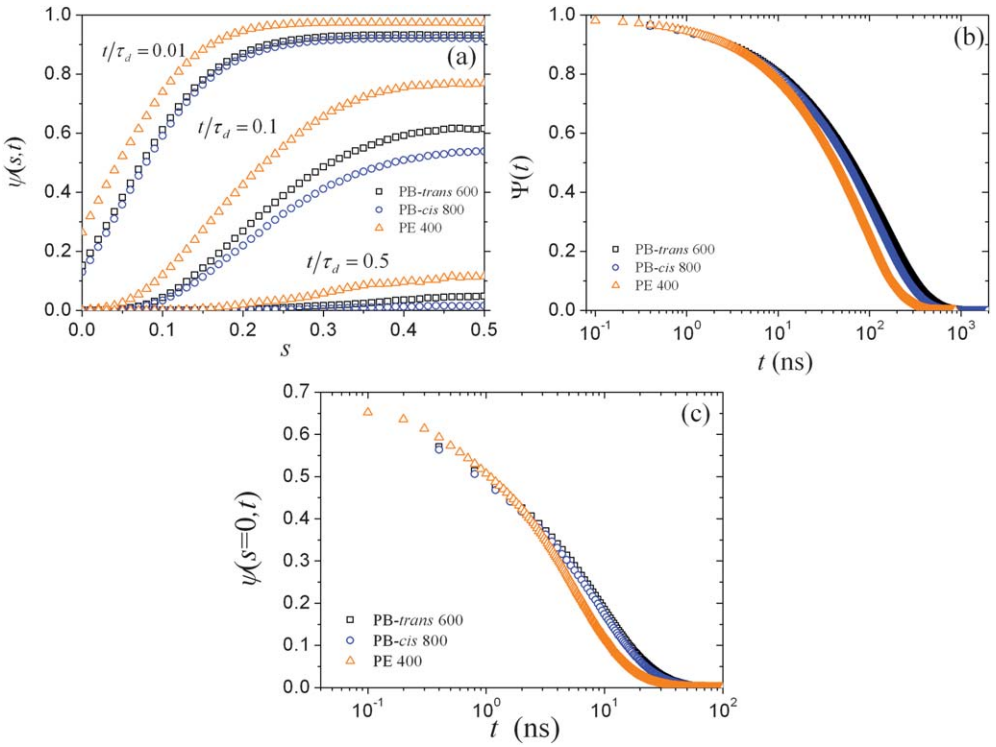


**Fig. 6** Relaxation curves for three different polymer melts (PE-400, PB-*cis*800 and PB-*trans*600) characterized though by the similar average number of entanglements $Z$ per chain ($5.33 \pm 1.15$, $5.04 \pm 0.93$, and $5.56 \pm 1.07$, respectively). (a) The segment survival probability function $\psi(s,t)$, (b) The average tube survival probability function $\Psi(t) \equiv \int_0^1 \psi(s,t)ds$, and (c) The end-segment survival probability function $\psi(s = 0,t)$ (or $\psi(s = 1,t)$).

theory, we have also considered the original Doi–Edwards model addressing chain relaxation in a static (fixed) network of obstacles. In the Appendix, we give a brief account of the four models.

In order to objectively assess the predictive capabilities of each model, the model parameters were determined directly based on the atomistic simulation data without introducing any empirical fitting, as follows: for the comparison of our PP simulation data with the original Doi–Edwards model for the PE500 melt, we used $\tau_d = 1042 \pm 46$ ns as determined from the atomistic msd[49] (see Table 1); for the comparison with the des Cloizeaux and Pattamaprom *et al.* models, we used $\tau_R = 125 \pm 20$ ns as estimated *via* the scaling $\tau_R \sim N^2$ based on the data of $\tau_R$ for a variety of shorter unentangled PE melts;[30,33,74] for the comparison with the Leygue *et al.* model, we used $X = 0.6$ and $\alpha = 1.0$, as proposed by these authors[21] based on a comparison with experimental data. All differential models were solved numerically with a Crank–Nicholson finite difference method,[75] by employing a segment (space) step $\Delta s$ in the interval [0,1] equal to $10^{-3}$ and a time step $\Delta\tilde{t}$ (in units of $\tilde{t} = t/(\pi^2\tau_d)$) equal to $10^{-7}$.

In Fig. 7, the four models are compared against the computed results from the direct PP analysis on the basis of their predictions for the $\psi(s,t)$ function at three different times (an early, an intermediate, and a late one on the order of the disentanglement time for the simulated system). According to the figure graphs: (a) The original Doi–Edwards model systematically overestimates $\psi(s,t)$ for all times; as expected, this is due to the fact that this model does not account for CLF or CR effects. (b) At relatively early times (*e.g.*, for $t = 0.01\tau_d$ in the figure), the predicted $\psi(s,t)$ from the three other models are below the computed data from the direct PP analysis; this is an indication that Doi's formula for CLF effects[14] (common in all of them) overestimates their contribution to the relaxation dynamics for the PE500 melt. (c) At progressively longer times (*e.g.*, for $t = 0.1\tau_d$), the effects of chain reptation and CR become more and more significant and this is captured rather well by the three models (the des Cloizeaux, Pattamaprom *et al.*, and Leygue *et al.* models). The Pattamaprom *et al.* and Leygue *et al.* models, in particular, give results that compare quite favourably (more favourable than the des Cloizeaux model) with the direct PP simulation data. (d) At even longer times (comparable to the disentanglement time for the system under study; *e.g.*, for $t = 0.35\tau_d$), the three models are seen to underestimate the overall relaxation dynamics, with the best agreement with the simulation data provided by the Pattamaprom *et al.* set of equations. Despite the inherent difficulties in theoretical approaches to the $\psi(s,t)$ function due to the multitude of relaxation phenomena present in an entangled polymer melt (especially, if it is weakly entangled), the comparison presented in Fig. 7 between the three models considered here and the computed PP curves is quite satisfactory, considering that no adjustment parameters were used.

Fig. 8 extends the comparison between the considered tube models and the direct PP analysis to the level of the overall tube survival probability function $\Psi(t)$. At early-to-intermediate time scales, the curves from the three models are below that from the direct PP analysis, emphasizing once more the overestimation of CLF and CR effects. Deviations between the three sets data and the PP analysis persist even at later times where we further observe that the curves corresponding to the des Cloizeaux and

 

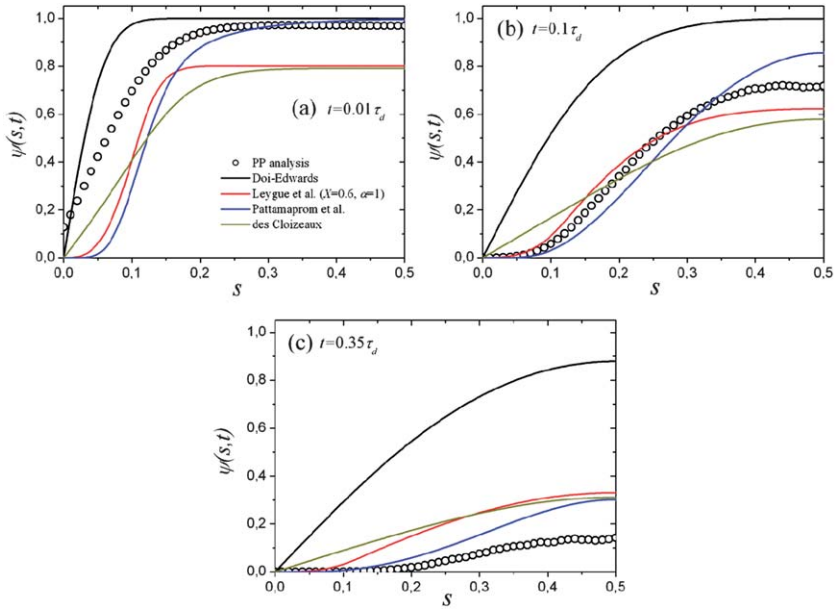


**Fig. 7** Comparison of the computed curves of the segment survival probability function $\psi(s,t)$ for the PE-500 system with the predictions of four tube models: the original Doi–Edwards model,[2] the Leygue *et al.* model,[21] the Pattamaprom *et al.* model,[23] and the des Cloizeaux model.[73] Data are shown at three different times: (a) an early, (b) an intermediate, and (c) a late.

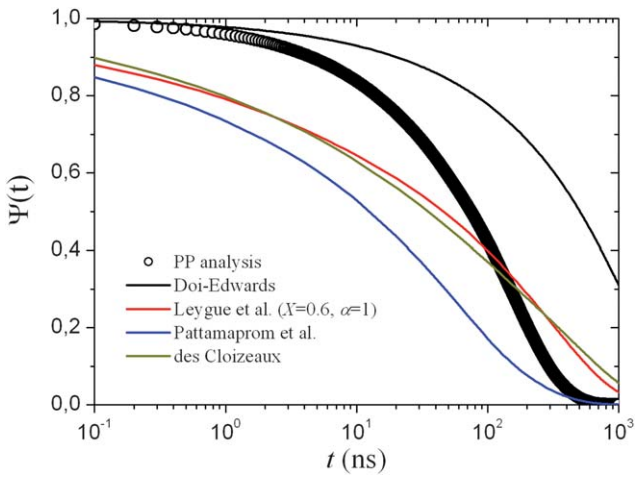


**Fig. 8** Same as with Fig. 7, but for the overall tube survival probability function $\Psi(t)$.

Leygue *et al.* models cross over the curve obtained from the PP analysis. Again, the best overall agreement with the computed PP data is offered by the Pattamaprom *et al.* model.

By Fourier transforming the computed $\Psi(t)$ data one can get predictions for the storage and loss moduli of the system under study. Thus, in Fig. 9 we present how the computed $G'(\omega)$ and $G''(\omega)$ spectra for the simulated PE500 melt from the direct PP analysis compare with the theoretical predictions. The largest deviations from the simulation results are exhibited by the original Doi–Edwards model due to the fact that CLF and CR effects are neglected in this model. The situation improves substantially with the modifications introduced in the new models correcting for both of these effects. More specifically, the Leygue *et al.* and des Cloizeaux models over-predict $G'(\omega)$ at low frequencies and slightly under-predict it at intermediate frequencies; this result is consistent with the predictions of the two models for $\Psi(t)$ discussed in Fig. 8. In contrast, the Pattamaprom *et al.* model under-predicts $G'(\omega)$ at both low and

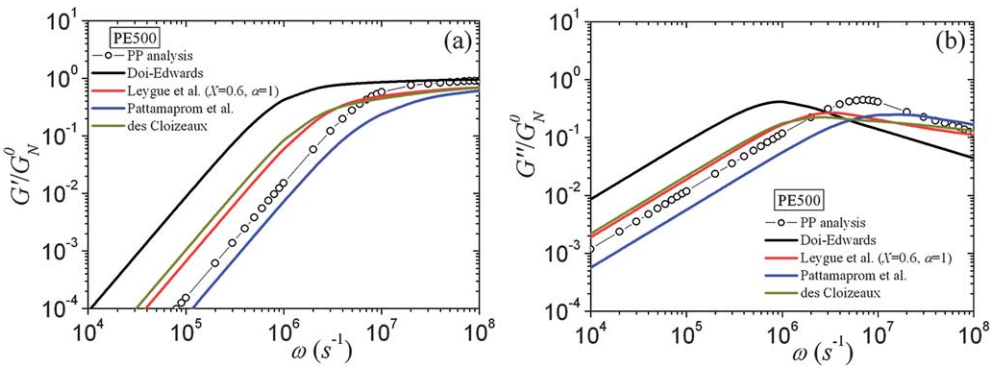


**Fig. 9** Same as with Fig. 7, but for: (a) the storage $G'(\omega)$, and (b) the loss modulus $G''(\omega)$.

intermediate frequencies, indicating that, overall, this model overestimates the combined CLF and CR effect. We can make similar comments by looking at the model predictions for $G''(\omega)$. In the main, however, and considering the lack of any adjustable parameters as well as the different ways with which the three analytical models correct for CR and CLF effects, the agreement between theoretical predictions and simulation data, although not perfect, seems quite promising.

## 5. Concluding remarks

Since the 1970s when de Gennes and Doi–Edwards introduced the first version of the tube model as a conceptual abstraction for capturing topological constraints for the dynamics of entangled polymers, the idea has been extensively explored, thereby resulting in the development of significant extensions capable of accounting for additional (to reptation) relaxation mechanisms present in the real system, such as contour length fluctuation and constraint release. In fact, as more experimental data has become available in recent years, new models have been subjected to numerous tests, which have demonstrated their ability to fit rheological data quite well in most cases, but discrepancies still exist. To aid in the development of even more accurate tube models we presented here a methodology capable of providing a molecular understanding of polymer melt dynamics by computing the most fundamental quantity of these models, the segment survival probability $\psi(s,t)$, which is extremely difficult (impossible at the moment) to measure experimentally. We have presented detailed results from such an approach for a variety of model PE and PB melts referring to a variety of issues. For example, we saw that:

- the value of the PP step length $a_s(=\langle R^2\rangle/\langle L\rangle)$ is approximately 15–40% larger than the value of the tube diameter $d_t$.

- both $\psi(s=0,t)$ and $\langle \mathbf{u}(s=0,t)\cdot\mathbf{u}(s=0,0)\rangle$ turn out to be non-zero for a finite time scale comparable to the characteristic chain entanglement time $\tau_e$.

- the simulation data are consistent with Doi's formula for CLFs (that $\Delta L/\langle L\rangle = XZ^{-1/2}$) with $0.5 \le X \le 0.7$ as suggested by des Cloizeaux[63] and Needs.[64]

- the simulation results for the time auto-correlation function of the PP contour length $L$ and the chain-end-to-end vector $\mathbf{R}$ are described better by a stretched-exponential or KWW function than by the weighted sum of an infinite series of exponential functions as predicted by the reptation theory; the correlation times of the auto-correlation functions of $L$ are about 30–50% smaller than the corresponding chain Rouse times for the PE and the *cis*-PB melts, and twice as large for the *trans*-PB systems.

The most appealing feature of our work is that the computed $\psi(s,t)$ curves can serve to test tube models at a more fundamental level than the one provided by the simple comparison against measured LVE data. We have demonstrated this here for four tube models: the original Doi–Edwards,[2,3] the des Cloizeaux,[73] the Leygue *et al.*,[21] and the Pattamaprom *et al.*[23] Such a test can: (a) evaluate the accuracy of expressions used to account for CLF and CR effects in the diffusion equation and suggest more accurate ones, (b) help investigate the range of conditions (*e.g.*, chain length and degree of polydispersity) over which these expressions are valid, and (c) elucidate the molecular origin of the proposed relaxation mechanisms (and even reveal new ones in certain cases).

We close this work by mentioning that the problem of chain dynamics in entangled polymer melts has been approached so far from two levels: theoretical (based on mesoscopic and continuum mechanics approaches) and experimental. Here, we have proposed approaching the problem from a third level, computational (molecular), which makes no unnecessary assumptions about the underlying relaxation mechanisms and avoids conceptual problems usually arising in theoretical treatments. We have described how one can extract the central quantity of the tube models and we have made an extensive comparison to four of them. We consider this as offering a more complete and detailed picture of the problem since we start from the molecular framework and project it onto the mesoscopic framework (primitive paths) on which phenomenological theories and approximate analytical expressions are based. Further extensions to systems such as polydisperse (*e.g.*, bidisperse) melts, branched polymers, and polymers under flowing conditions,[76] would be valuable. Work is currently under way along these directions.

## Appendix: a brief account of the four models employed in comparison to the PP analysis

In this appendix we summarize the four tube models (by Doi–Edwards, des Cloizeaux, Pattamaprom *et al.*, and Leygue *et al.*) that are used in comparison with the results from the PP analysis (Figs 7–9).

### The Doi–Edwards model

In the original Doi–Edwards model,[2] the function $\psi(s,t)$ obeys the diffusion equation:

$$\frac{\partial\psi(x,t)}{\partial t} = D_c\frac{\partial^2\psi(x,t)}{\partial x^2} \tag{A1a}$$

subject to the following set of initial and boundary conditions

$$\begin{aligned}\psi(x,t=0) &= 1\\ \psi(x=0,t) &= \psi(x=L,t) = 0\end{aligned} \tag{A1b}$$

with $x \in [0,L]$. The boundary conditions reflect the idea that chain ends relax instantaneously, something that contradicts the findings of our PP analysis (see, *e.g.*, Figs. 4(a) and 5(a)). As we discussed above, the same assumption accompanies the majority of existing tube models (most probably for reasons of mathematical simplicity), but the recent work of Ruymbeke *et al.*[71] demonstrated that the effect of a finite relaxation time for chain ends can make an important difference in the comparison with experimental data. The above equations can be simplified by writing them in the form:

$$\frac{\partial\psi(s,\tilde{t})}{\partial\tilde{t}} = \frac{\partial^2\psi(s,\tilde{t})}{\partial s^2} \tag{A1c}$$

with initial and boundary conditions that:

$$\begin{aligned}\psi(s,\tilde{t}=0) &= 1\\ \psi(s=0,\tilde{t}) &= \psi(s=1,\tilde{t}) = 0\end{aligned} \tag{A1d}$$



 

by using the following dimensionless variables: $\tilde{t} = t/(\pi^2\tau_d)$ with $\tau_d = L^2/(\pi^2 D_c)$, and $s = x/L$. Eqns (A1c and d) admit the following analytical solution:

$$\psi(s,t) = \sum_{p;\mathrm{odd}} \frac{4}{p\pi}\sin(p\pi s)\exp\left(-\frac{p^2 t}{\tau_d}\right) \tag{A1e}$$

implying also that:

$$\Psi(t) = \int_0^1 ds\psi(s,t) = \sum_{p;\mathrm{odd}} \frac{8}{(p\pi)^2}\exp\left(-\frac{p^2 t}{\tau_d}\right) \tag{A1f}$$

### The des Cloizeaux model

The des Cloizeaux model[73] incorporates a time-dependent diffusion coefficient into the diffusion equation by considering the early-time (*e.g.*, $t < \tau_R$) Rouse dynamics of the primitive chain segments. Although, in the original treatment, des Cloizeaux used in the diffusion equation for simplicity not $D_c(x,t)$ itself but its average over $x$, *i.e.*, $D_c(t)$, in the present work we have directly employed $D_c(x,t)$; thus the corresponding diffusion equation reads:

$$\frac{\partial\psi''(s,t)}{\partial t} = \frac{1}{L^2}\frac{\partial}{\partial s}\left(D_c(s,t)\frac{\partial\psi''(s,t)}{\partial s}\right) \tag{A2a}$$

with

$$D_c(s,t) = D_c\left[1 + 2\sum_{p=1}^{\infty}\cos^2(p\pi s)\exp\left(-tp^2/\tau_R\right)\right] \tag{A2b}$$

subject to the same initial and boundary conditions as the Doi–Edwards model, eqn (A1b) or (A1d) above. After solving for $\psi''(s,t)$ from eqns (A2a) and (A2b), the segment survival probability function is obtained by making use of the notion of double reptation,[26] that is, as:

$$\psi(s,t) = \psi''(s,t)\int_0^1 ds\,\psi''(s,t) \tag{A2c}$$

Thus leading to the double reptation model:

$$\Psi(t) = \left(\int_0^1 ds\psi''(s,t)\right)^2; \quad G(t) = G_N^0\Psi(t) \tag{A2d}$$

### The Pattamaprom *et al.* model

The Pattamaprom *et al.* model[23] (also called the dual constraint model) solves the diffusion equation in two stages. In the first stage, the diffusion equation incorporates only chain reptation and CLF effects but omits CR (*i.e.*, it initially considers chain motion in a fixed tube):

$$\frac{\partial}{\partial t}\psi^*(s,t) = \frac{D_c}{L^2}\frac{\partial^2}{\partial s^2}\psi^*(s,t) - \frac{1}{\tau^*(s)}\psi^*(s,t) \tag{A3a}$$

where

$$\begin{aligned}\tau_{\mathrm{early}}(s) &= \frac{9}{16}\pi^3\frac{\tau_R}{c^4}Z^2(1-cs)^4\\ \tau^*_{\mathrm{late}}(s) &= \frac{\tau_R}{c^2}\exp\left[U^*(s)\right]\\ U^*(s) &= \tfrac{3}{2}Z(1-cs)^2\end{aligned} \tag{A3b}$$

subject to the usual initial and boundary conditions, eqn (A1b) or eqn (A1d) above. Here $c$ is equal to 2 for a linear chain. The expressions for the early- and late-time CLF effects have been taken from the works of Doi[14] and Milner–McLeish,[77] respectively. $\tau^*(s)$, on the other hand, is given by

$$\tau^*(s) = \begin{cases}\tau_{\mathrm{early}}(s) & \text{for } (1-cs) < C_1^*\\ \sqrt{\tau_{\mathrm{early}}(s)\tau^*_{\mathrm{late}}(s)} & \text{for } C_1^* < (1-cs) < C_2^*\\ \tau^*_{\mathrm{late}}(s) & \text{for } (1-cs) < C_2^*\end{cases} \tag{A3c}$$

where $C_1^*$ denotes the segment position close to the chain ends, corresponding to the first crossover of $\tau_{\mathrm{early}}$ to $\tau^*_{\mathrm{late}}$ (*i.e.*, $(1-cs) = 0$) and $C_2^*$ the segment position for the second crossover of $\tau_{\mathrm{early}}$ to $\tau^*_{\mathrm{late}}$ deeper inside the tube. The overall tube survival probability is obtained by integrating $\psi^*(s,t)$ over $s$, *i.e.*, as $\phi^*(t) = \int_0^1 ds\psi^*(s,t)$, and we compute the average probability $\Phi^*(t)$ as:

$$\Phi^*(t) = \begin{cases}\phi^*(t) \text{ if } \phi^*(t) > \phi_R^*(t)\\ \phi_R^*(t) \text{ if } \phi^*(t) < \phi_R^*(t)\end{cases} \tag{A3d}$$

after we compare $\phi^*(t)$ with the following approximate Rouse process

$$\phi_R^*(t) = \phi^*(t_0)\left(\frac{t}{t_0}\right)^{-1/2} \tag{A3e}$$

where $t_0$ is the time when $\phi^*(t)$ starts to decrease faster than $t^{-1/2}$.

In the second stage, the computed $\Phi^*(t)$ function is employed in the expression for the activation energy $U(s)$ for chain retraction in deep fluctuations, $\tau_{\mathrm{late}}(s)$, to account for the CR effect. The equations corresponding to (A3a) and (A3b) are then

$$\frac{\partial}{\partial t}\psi(s,t) = \frac{D_c}{L^2}\frac{\partial^2}{\partial s^2}\psi(s,t) - \frac{1}{\tau(s)}\psi(s,t) \tag{A3f}$$

with

$$\begin{aligned}\tau_{\mathrm{early}}(s) &= \frac{9}{16}\pi^3\frac{\tau_R}{c^4}Z^2(1-cs)^4\\ \tau_{\mathrm{late}}(s) &= \frac{\tau_R}{c^2}\exp[U(s)]\\ U(s) &= \frac{3}{2}Z\Phi^*(t)(1-cs)^2\end{aligned} \tag{A3g}$$

respectively. We see that $\tau_{\mathrm{early}}$ is given by the same equation as eqn (A3b) above. $\tau(s)$, on the other hand, is obtained in a way that is analogous to that in the first stage, *i.e.*, as

$$\tau(s) = \begin{cases}\tau_{\mathrm{early}}(s) & \text{for } (1-cs) < C_1\\ \sqrt{\tau_{\mathrm{early}}(s)\tau_{\mathrm{late}}(s)} & \text{for } C_1 < (1-cs) < C_2\\ \tau_{\mathrm{late}}(s) & \text{for } (1-cs) < C_2\end{cases} \tag{A3h}$$

with the parameters $C_1$ and $C_2$ denoting again the crossover points; however, since now $\Phi^*(t)$ is included in $\tau_{\mathrm{late}}$, their values are time-dependent. Solving for $\psi(s,t)$ allows one to compute first the overall probability $\phi(t) = \int_0^1 ds\psi(s,t)$ and then the average probability $\Phi(t)$ as:

$$\Phi(t) = \begin{cases}\phi(t) \text{ if } \phi(t) > \phi_R(t)\\ \phi_R(t) \text{ if } \phi(t) < \phi_R(t)\end{cases} \tag{A3i}$$

by comparing again $\phi(t)$ with the approximate Rouse process

$$\phi_R(t) = \phi(t_0)\left(\frac{t}{t_0}\right)^{-1/2} \tag{A3j}$$

where $t_0$ is the time when $\phi(t)$ starts to decrease faster than $t^{-1/2}$. Adopting the concept of double reptation,[26] the overall tube survival probability $\Psi(t)$ which enters the calculation of the relaxation modulus through $G(t) = G_N^0\Psi(t)$ is eventually given by:

$$\Psi(t) = \Phi(t)\phi(t) \tag{A3k}$$

### The Leygue *et al.* model

The Leygue *et al.* model[21] is represented by the following modified diffusion equation:

$$\frac{\partial\psi(s,t)}{\partial t} = \frac{1}{L^2}\frac{\partial}{\partial s}\left(D_c(s)\frac{\partial\psi(s,t)}{\partial s}\right) + \beta(t;\alpha)\psi(s,t) \tag{A4a}$$

with

$$\beta(t;\alpha) = \alpha\frac{\frac{1}{\pi^2\tau_d}\int_0^1 ds\frac{\partial}{\partial s}\left(D_c(s)\frac{\partial\psi(s,t)}{\partial s}\right)}{\int_0^1\psi(s,t)ds} \tag{A4b}$$

subject to the same initial and boundary conditions as eqn (A1b) or eqn (A1d) above. Eqn (A4a) with the form for $\beta(t;\alpha)$ prescribed by eqn (A4b) leads to a solution for $\psi(s,t)$ of the form:

$$\psi(s,t) = \psi'(s,t)(\int_0^1 ds\psi'(s,t))^{\alpha};\ G(t) = G_N^0\Psi(t) \tag{A4c}$$

with $\psi'(s,t)$ being the solution of the following diffusion equation without CR effects:

$$\frac{\partial\psi'(s,t)}{\partial t} = \frac{1}{L^2}\frac{\partial}{\partial s}\left(D_c(s)\frac{\partial\psi'(s,t)}{\partial s}\right) \tag{A4d}$$

In eqn (A4c), the choice $\alpha = 1$ corresponds to double reptation.[26] The expression for the curvilinear diffusion coefficient $D_c(s)$ employed in the model is that proposed by Doi:[14]

$$D_c(s) = \begin{cases} \dfrac{X^2}{Zs^2} & \text{for } s < \dfrac{X}{\sqrt{Z}} \\ \dfrac{X^2}{Z(1-s)^2} & \text{for } s > 1 - \dfrac{X}{\sqrt{Z}} \\ 1 \quad \text{otherwise} & \end{cases} \tag{A4e}$$

with $X$ and $\alpha$ undetermined numerical (*i.e.*, fitting) parameters.

## Acknowledgements

We are grateful to Dr Georgia Tsolou and Prof. Martin Kröger for their help with the generation of the atomistic trajectories for the PB-*trans*600 and PB-*cis*600 melts and the subsequent PP analysis, respectively. We acknowledge the support provided by: (a) the European Commission through the MODIFY (FP7-NMP-2008-SMALL-2, Code 228320) research project, and (b) the National Science Foundation (USA) under Grant No. CBET-0742679 through the resources of the PolyHub Virtual Organization.

## References

1 P. G. de Gennes, *J. Chem. Phys.*, 1971, **55**, 572.
2 M. Doi and S. F. Edwards, *J. Chem. Soc., Faraday Trans. 2*, 1978, **74**, 1789; M. Doi and S. F. Edwards, *J. Chem. Soc., Faraday Trans. 2*, 1978, **74**, 1802; M. Doi and S. F. Edwards, *J. Chem. Soc., Faraday Trans. 2*, 1978, **74**, 1818.
3 M. Doi and S. F. Edwards, *The Theory of Polymer Dynamics*, Clarendon Press, Oxford, 1986.
4 S. F. Edwards, *Proc. Phys. Soc.*, 1967, **92**, 9.
5 S. F. Edwards, *Polymer*, 1977, **9**, 140.
6 J. D. Ferry, *Viscoelastic Properties of Polymers*, John Wiley & Sons, New York, 1980.
7 W. W. Graessley, *Adv. Polym. Sci.*, 1974, **16**, 1.
8 T. P. Lodge, *Phys. Rev. Lett.*, 1999, **83**, 3218.
9 M. Baumgaertel, A. Schausberger and H. H. Winter, *Rheol. Acta*, 1990, **29**(5), 400; M. Baurngaertel, M. E. De Rosa, J. Machado, M. Masse and H. H. Winter, *Rheol. Acta*, 1992, **31**(1), 75.
10 S. T. Milner and T. C. B. McLeish, *Phys. Rev. Lett.*, 1998, **81**, 725.
11 T. C. B. McLeish, *Adv. Phys.*, 2002, **51**, 1379.
12 W. W. Graessley, *J. Polym. Sci., Polym. Phys. Ed.*, 1980, **18**, 27.
13 H. Watanabe, *Prog. Polym. Sci.*, 1999, **24**, 1253.
14 M. Doi, *J. Polym. Sci., Polym. Lett. Ed.*, 1981, **19**(5), 265; M. Doi, *J. Polym. Sci., Polym. Phys. Ed.*, 1983, **21**(5), 667.
15 S. F. Edwards and J. W. V. Grant, *J. Phys. A: Math., Nucl. Gen.*, 1973, **6**, 1169; P. G. de Gennes, *J. Phys.*, 1975, **36**, 1199; P. G. de Gennes, *Macromolecules*, 1976, **9**, 587; J. Klein, *Macromolecules*, 1978, **11**, 852.
16 A. Wischnewski, M. Monkenbusch, L. Willner, D. Richter, A. E. Likhtman, T. C. B. McLeish and B. Farago, *Phys. Rev. Lett.*, 2002, **88**, 058301.
17 M. Rubinstein and R. H. Colby, *J. Chem. Phys.*, 1988, **89**, 5291.
18 M. Doi, W. W. Graessley, E. Helfand and D. S. Pearson, *Macromolecules*, 1987, **20**, 1900.
19 J. L. Viovy, M. Rubinstein and R. H. Colby, *Macromolecules*, 1991, **24**, 3587.
20 J. des Cloizeaux, *Macromolecules*, 1990, **23**, 3992.
21 A. Leygue, C. Bailly and R. Keunings, *J. Non-Newtonian Fluid Mech.*, 2006, **133**, 28.
22 R. S. Graham, A. E. Likhtman, T. C. B. McLeish and S. T. Milner, *J. Rheol.*, 2003, **47**, 1171.
23 C. Pattamaprom, R. G. Larson and T. J. Van Dyke, *Rheol. Acta*, 2000, **39**, 517; C. Pattamaprom and R. G. Larson, *Rheol. Acta*, 2001, **40**, 516.
24 C. Pattamaprom, R. G. Larson and A. Sirivat, *Rheol. Acta*, 2008, **47**, 689.
25 J. Koga, K. Kimura and S. Homma, *Chem. Eng. Sci.*, 2007, **62**, 2330.
26 J. L. Viovy, *J. Phys.*, 1985, **46**, 847; G. Marrucci, *J. Polym.Sci., Polym. Phys. Ed.*, 1985, **23**, 159; C. Tsenoglou, *ACS Polym. Prepr.*, 1987, **28**, 185; J. des Cloizeaux, *Europhys. Lett.*, 1988, **5**, 437.
27 R. H. Colby and M. Rubinstein, *Macromolecules*, 1990, **23**, 2753.
28 R. H. Colby, L. J. Fetters and W. W. Graessley, *Macromolecules*, 1987, **20**, 2226.
29 M. P. Allen and D. J. Tildesley, *Computer Simulation of Liquids*, Clarendon Press, Oxford, 1987.
30 V. A. Harmandaris, V. G. Mavrantzas, D. N. Theodorou, M. Kröger, J. Ramírez, H. C. Öttinger and D. Vlassopoulos, *Macromolecules*, 2003, **36**, 1376.
31 G. Tsolou, V. G. Mavrantzas and D. N. Theodorou, *Macromolecules*, 2005, **38**, 1478.
32 D. J. Evans and G. P. Morriss, *Statistical Mechanics of Nonequilibrium Liquids*, Academic Press, New York, 1990.
33 C. Baig, B. J. Edwards, D. J. Keffer and H. D. Cochran, *J. Chem. Phys.*, 2005, **122**, 184906; C. Baig, B. J. Edwards, D. J. Keffer, H. D. Cochran and V. A. Harmandaris, *J. Chem. Phys.*, 2006, **124**, 084902.
34 R. Ketzmerick and H. C. Öttinger, *Continuum Mech. Thermodyn.*, 1989, **1**, 113.
35 K. Kremer and G. S. Grest, *J. Chem. Phys.*, 1990, **92**, 5057.
36 M. Kröger, *Phys. Rep.*, 2004, **390**, 453.
37 W. Tschöp, K. Kremer, J. Batoulis, T. Buerger and O. Hahn, *Acta Polym.*, 1998, **49**, 61; W. Tschöp, K. Kremer, O. Hahn, J. Batoulis and T. Buerger, *Acta Polym.*, 1998, **49**, 75.
38 V. A. Harmandaris, N. P. Adhikari, N. F. A. Van der Vegt and K. Kremer, *Macromolecules*, 2006, **39**, 6708; V. A. Harmandaris and K. Kremer, *Macromolecules*, 2009, **42**, 791.
39 J. T. Padding and W. J. Briels, *J. Chem. Phys.*, 2002, **117**, 925; J. T. Padding and W. J. Briels, *J. Chem. Phys.*, 2003, **118**, 10276.



 

40 D. Reith, M. Pütz and F. Müller-Plathe, *J. Comput. Chem.*, 2003, **24**, 1624; H.-J. Qian, P. Carbone, X. Chen, H. Al Karimi-Verzaneh, C. C. Liew and F. Müller-Plathe, *Macromolecules*, 2008, **41**, 9919; H.-J. Qian, C. C. Liew and F. Müller-Plathe, *Phys. Chem. Chem. Phys.*, 2009, **11**, 1962.
41 T. Spyriouni, C. Tzoumanekas, D. N. Theodorou, F. Müller-Plathe and G. Milano, *Macromolecules*, 2007, **40**, 3876.
42 Y. Masubuchi, J. Takimoto, K. Koyama, G. Ianniruberto, G. Marrucci and F. Greco, *J. Chem. Phys.*, 2001, **115**, 4387; Y. Masubuchi, G. Ianniruberto, F. Greco and G. Marrucci, *J. Chem. Phys.*, 2003, **119**, 6925; Y. Masubuchi, G. Ianniruberto, F. Greco and G. Marrucci, *Modell. Simul. Mater. Sci. Eng.*, 2004, **12**, S91.
43 D. M. Nair and J. D. Schieber, *Macromolecules*, 2006, **39**, 3386.
44 C. Baig and V. A. Harmandaris, *Macromolecules*, 2010, **43**, 3156.
45 R. Everaers, S. K. Sukumaran, G. S. Grest, C. Svaneborg, A. Sivasubramanian and K. Kremer, *Science*, 2004, **303**, 823.
46 M. Kröger, *Comput. Phys. Commun.*, 2005, **168**, 209.
47 K. Foteinopoulou, N. C. Karayiannis, V. G. Mavrantzas and M. Kröger, *Macromolecules*, 2006, **39**, 4207.
48 C. Tzoumanekas and D. N. Theodorou, *Macromolecules*, 2006, **39**, 4592.
49 P. S. Stephanou, C. Baig, G. Tsolou, V. G. Mavrantzas and M. Kröger, *J. Chem. Phys.*, 2010, **132**, 124904.
50 C. Baig and V. G. Mavrantzas, *Soft Matter*, 2010, DOI: 10.1039/b916054j.
51 M. Doi, *J. Phys. A: Math. Gen.*, 1975, **8**, 959.
52 C. Baig, P. S. Stephanou and V. G. Mavrantzas, unpublished work.
53 N. C. Karayiannis and V. G. Mavrantzas, *Macromolecules*, 2005, **38**, 8583.
54 L. J. Fetters, D. J. Lohse, D. Richter, T. A. Witten and A. Zirkel, *Macromolecules*, 1994, **27**, 4639.
55 J. C. Horton, G. L. Squires, A. T. Boothroyd, L. J. Fetters, A. R. Rennie, C. J. Glinka and R. A. Robinson, *Macromolecules*, 1989, **22**, 681.
56 L. J. Fetters, W. W. Graessley, R. Krishnamoorti and D. J. Lohse, *Macromolecules*, 1997, **30**, 4973.
57 N. Hadjichristidis, X. Zhongde, L. J. Fetters and J. Roovers, *J. Polym. Sci., Polym. Phys. Ed.*, 1982, **20**, 743.
58 Y.-H. Lin, *Macromolecules*, 1987, **20**, 3080.
59 L. J. Fetters, D. J. Lohse and W. W. Graessley, *J. Polym. Sci., Part B: Polym. Phys.*, 1999, **37**, 1023.
60 L. J. Fetters, D. J. Lohse, S. T. Milner and W. W. Graessley, *Macromolecules*, 1999, **32**, 6847.
61 D. J. Lohse, *J. Macromol. Sci., Part C*, 2005, **45**, 289.
62 H. C. Öttinger, *J. Non-Newtonian Fluid Mech.*, 2004, **120**, 207.
63 J. des Cloizeaux, *J. Phys., Lett.*, 1984, **45**, L17.
64 R. J. Needs, *Macromolecules*, 1984, **17**, 437.
65 R. Ketzmerick and H. C. Öttinger, *Continuum Mech. Thermodyn.*, 1989, **1**, 113.
66 S. Shanbhag and R. G. Larson, *Phys. Rev. Lett.*, 2005, **94**, 076001.
67 C. Y. Liu, J. He, R. Keunings and C. Bailly, *Macromolecules*, 2006, **39**, 3093; C. Y. Liu, J. He, E. van Ruymbeke, R. Keunings and C. Bailly, *Polymer*, 2006, **47**, 4461.
68 M. Abramowitz and I. A. Stegun, *Handbook of Mathematical Functions*, National Bureau of Standards, Washington, 1964.
69 M. Kröger and S. Hess, *Phys. A*, 1993, **195**, 336.
70 T. Aoyagi and M. Doi, *Comput. Theor. Polym. Sci.*, 2000, **10**, 317.
71 E. van Ruymbeke, D. Vlassopoulos, M. Kapnistos, C. Y. Liu and C. Bailly, *Macromolecules*, 2010, **43**, 525.
72 G. Tsolou and V. G. Mavrantzas, in Applications of Molecular Systems Engineering, ed. C. S. Adjiman and A. Galindo, Wiley-VCH, 2010, *Process Systems Engineering*: vol. 6, pp. 85–134.
73 J. des Cloizeaux, *Macromolecules*, 1990, **23**, 4678.
74 V. G. Harmandaris, V. G. Mavrantzas and D. N. Theodorou, *Macromolecules*, 1998, **31**, 7934.
75 W. H. Press, S. A. Tevkolsky and B. P. Flannery, *Numerical Recipes in Fortran 77*, Cambridge University Press, Cambridge, 1992.
76 G. Marrucci, *J. Non-Newtonian Fluid Mech.*, 1996, **62**, 279; G. Ianniruberto and G. Marrucci, *J. Non-Newtonian Fluid Mech.*, 1996, **65**, 241.
77 S. T. Milner and T. C. B. McLeish, *Macromolecules*, 1997, **30**, 2159.